Sustainable Energy & Fuels

ROYAL SOCIETY OF CHEMISTRY

PAPER

View Article Online
View Journal | View Issue



Cite this: *Sustainable Energy Fuels*, 2022, **6**, 3830

# Flexible methanol and hydrogen production from biomass gasification with negative emissions†

Alessandro Poluzzi, Giulio Guandalini and Matteo C. Romano *

Bioenergy plants with carbon capture and storage have been recently receiving attention as negative emission technologies. In this work, a techno-economic analysis of bio-methanol and bio-hydrogen production plants coupled with carbon capture and storage is conducted. The plants include different gasification technologies (direct oxygen-blown gasification and indirect gasification) and different $CO_2$ capture processes (pre-combustion MDEA-based and post-combustion MEA-based $CO_2$ capture) from different streams, to achieve increasing $CO_2$ capture rates at increasing marginal costs. Moreover, an assessment of the economic impact of multi-product plants which flexibly produce methanol and hydrogen is carried out. Overall fuel production efficiencies of between 65.1 and 68.1% have been computed in all cases, showing a little dependency of energy efficiency on the gasification technology and the final product. In methanol production plants, a $CO_2$ capture rate of between 26 and 55%, depending on the gasification technology, can be reached *via* a pre-combustion capture process at a cost of 41–46 € per $t_{CO_2}$. In hydrogen production plants, between 64 and 90% capture efficiency can be reached at a cost of 52–56 € per $t_{CO_2}$. Higher $CO_2$ capture efficiency, resulting in $CO_2$ residual emissions below 2% of the inlet carbon, can be achieved *via* post-combustion capture with a marginal cost of 98–205 € per $t_{CO_2}$ and an average cost of 47–77 € per $t_{CO_2}$. Flexible methanol-$H_2$ production plants result in the highest capex and the highest LCOF. However, when considering the time-dependent $H_2$ market price, the internal rate of return of flexible methanol-$H_2$ plants is slightly higher or slightly lower than that of the corresponding best single-product plant. On the other hand, multi-product flexible plants are never the worst case scenario despite the highest investment costs, thus offering a potential advantage from the financial risk perspective thanks to lower exposure to market price volatility.

Received 11th May 2022
Accepted 6th July 2022

DOI: 10.1039/d2se00661h

rsc.li/sustainable-energy



## 1. Introduction

Hydrogen production from biogenic feedstocks has been recently receiving attention due to (i) the high added value of the final product which offers opportunities for the decarbonisation of a wide range of sectors (*e.g.* long-haul transport, high temperature industrial heating, chemicals, iron and steel), and to (ii) the possibility of providing negative emissions by capturing and storing the $CO_2$ which is produced within the conversion process (*i.e.* bioenergy with carbon capture and storage –BECCS–). For this reason, biomass-to-hydrogen ($BtH_2$) plants with carbon capture and storage (CCS) are included in a broader spectrum and scenario analyses as a key option to meet $CO_2$ emission reduction objectives.

Baker *et al.*[1] investigated several BECCS pathways which may allow California to reach the target of carbon neutrality by 2045. The $BtH_2$ pathway *via* biomass gasification shows the lowest $CO_2$ removal cost (25–57 € per $t_{CO_2}$) among all the analysed technologies (*e.g.* direct air capture, biogas-to-electricity, fast pyrolysis, *etc.*). The cost significantly depends on the type and on the origin of the inlet biomass. $BtH_2$ plants guarantee a high capture rate, as up to 95% of the carbon contained in the feedstock can be captured.

Bui *et al.*[2] analysed the potential to meet negative emission targets of a series of BECCS plants, among which there are more mature technologies such as biomass-fired power plants and biomass-fuelled combined heat and power plants, and less mature ones such as $BtH_2$ plants. The report showed that $BtH_2$ can play a major role in meeting $CO_2$ removal targets and that it is more cost-effective to deploy $BtH_2$ plants alongside more mature BECCS technologies (*e.g.* biomass-fuelled combined heat and power plants).

Hannula *et al.*[3] examined the potential of carbon-neutral synthetic fuels (*i.e.* biofuel *via* gasification and electrofuels from $CO_2$ and water using electricity) in decarbonizing road transport. Synthetic fuel plants are expected to have advantages in long-haul light duty and/or heavy duty options where battery operated electric vehicles are less competitive. According to the International Energy Agency (IEA), 26 EJ $year^{-1}$ of biofuels

*P, olitecnico di Milano, Department of Energy, Via Lambruschini 4, 20156 Milano, Italy. E-mail: matteo.romano@polimi.it*

† Electronic supplementary information (ESI) available. See https://doi.org/10.1039/d2se00661h

would be consumed globally in the transportation sector in 2050.[4] BECCS plants may cover that consumption in the most effective way, ensuring higher emission savings than biofuel plants without CCS and electrofuels. BECCS plants can not only produce negative emissions, but are also less sensitive to power sector emissions and they are not dependent on scarce low-carbon electricity which may limit the deployment of several technologies in the future.

The most significant techno-economic analyses in the scientific literature about $BtH_2$ plants are summarised in Table 1. The reported studies are mainly focused on large plants (*i.e.* 100–1700 MW of biomass input) where, in some cases, biomass is co-fed with coal, and different gasification technologies are considered, such as oxygen-blown fluidized bed, indirect dual fluidized bed, and entrained flow oxygen-blown gasification.

Larson *et al.*[5] investigated large-scale gasification-based systems for producing different biofuels, namely Fischer–Tropsch (F–T) fuels, dimethyl ether (DME) and hydrogen. In the hydrogen production plant, biomass is gasified in an oxygen-blown fluidized bed reactor for producing syngas. Two sour shift reactors and $CO_2$ separation with Rectisol allow for maximising the production of hydrogen in the downstream pressure swing adsorption (PSA) system. The biomass-to-hydrogen process proves to be the most fuel efficient among all the analysed cases (about 59%). From an economic perspective, the costs of production are relatively low, favoured by the large size of the plants (*i.e.* 13.6 € per GJ for 893 MW of biomass input). The cost of producing hydrogen is the lowest (per GJ) among all the fuels examined in the article. The possibility of adding CCS to the plant was not investigated.

Salkuyeh *et al.*[6] performed a techno-economic analysis of $BtH_2$ plants with and without CCS employing two different gasification technologies, namely dual fluidized bed indirect steam gasification and oxygen-blown entrained flow gasification. The entrained flow reactor allows the downstream syngas reforming and tar removal to be avoided, but it increases the plant complexity and capital cost. The syngas conditioning section is composed of high-temperature and low-temperature water-gas shift (WGS) reactors in series, placed downstream of sulphur cleaning, and of MDEA-based scrubbing as a $CO_2$ removal unit. Hydrogen is produced through PSA. When CCS is included, the oxy-combustion of PSA tail gas is carried out. When CCS is included, steam and electricity produced by exploiting PSA tail gas are not sufficient to satisfy the internal demand, and therefore additional natural gas is burned (3–8% of biomass input power) in order to increase steam and electricity production. The entrained flow gasification-based plant with CCS can capture almost all the $CO_2$ produced during the process. Conversely, the dual fluidized bed option captures only 60% of the produced $CO_2$ since only the $CO_2$ contained in the syngas is captured and the $CO_2$ from the combustor is emitted. The entrained flow gasification-based plant allows a higher fuel efficiency to be achieved compared to the fluidised bed option (47.5% *vs.* 37.6%). It is important to highlight that the obtained fuel efficiencies are significantly lower than those reported in other articles for similar gasification technologies. The reason for such low efficiencies cannot be derived from the information in the article. Although the two plant configurations with CCS share the same hydrogen production cost, the integration of CCS is less costly in the case of the entrained flow gasification-based plant (6.6 € per $t_{CO_2}$ *vs.* 9.1 € per $t_{CO_2}$).

Antonini *et al.*[7] conducted a techno-environmental analysis of $BtH_2$ plants based on three different gasification technologies, namely indirect dual fluidized bed steam gasification (heat pipe reformer), sorption-enhanced oxygen-blown gasification and oxygen-blown entrained flow gasification. The heat pipe reforming and sorption-enhanced gasification-based plants share similar units downstream of the gasification section, that include steam methane reforming, externally heated by the combustion of PSA tail gas, and a high-temperature WGS reactor. The entrained-flow gasification-based plant, instead, does not need syngas reforming, but it includes a low-temperature WGS reactor, downstream of the high-temperature one, in order to convert the high amount of CO contained in the syngas. In all the configurations, $CO_2$ is removed through MDEA scrubbing and hydrogen is produced in a PSA unit. The biofuel plants are studied with and without CCS. When CCS is not included, the MDEA scrubbing unit is not present. Oxy-combustion within the combustor of the dual fluidized bed sorption-enhanced gasification-based plant guarantees additional $CO_2$ capture. Sorption-enhanced and heat pipe reformer gasification-based plants are more fuel efficient than the entrained flow option, which requires more biomass per unit of hydrogen produced due to biomass energy loss in the pre-treatment process and less efficient gasification process. In contrast, the entrained-flow gasification-based plant can achieve the highest $CO_2$ capture rate (*i.e.* 98%), since steam methane reforming is not needed and related emissions from tail gas combustion are avoided. The sorption-enhanced configuration can achieve up to a 92% $CO_2$ capture rate by combining MDEA scrubbing with the oxy-combustion within the gasification section. The heat pipe reforming gasification option only achieves a 60% $CO_2$ capture rate, since a post-combustion $CO_2$ removal technology is not employed for the flue gas exiting the gasification section.

Del Pozo *et al.*[8] investigated the techno-economic potential of hydrogen production from large-scale coal/biomass (biomass $30\%_{wt}$) co-gasification plants with $CO_2$ capture. A benchmark plant is compared with three other plant configurations. The benchmark plant includes oxygen-blown entrained flow gasification, two sour-shift reactors, $CO_2$ removal with Selexol, PSA for hydrogen purification and a steam cycle. All the other plant configurations include entrained flow oxygen-blown gasification, high-temperature WGS reactors and membrane-assisted WGS, which replaces the Selexol absorption and the PSA unit. The first configuration produces power through oxy-combustion of the membrane-assisted WGS retentate to generate additional steam for the steam turbine. The second plant configuration introduces a more efficient entrained-flow gasification with slurry vaporization and power generation with a gas turbine fuelled by the purge stream of the $CO_2$ cryogenic purification unit. The third configuration removes the power cycle, allowing for electricity imports and performing oxy-combustion of the retentate in order to increase steam

production and therefore hydrogen production. All the proposed configurations are proven to be more fuel efficient than the benchmark (62.9–73% *vs.* 59.3%) and with a higher or very close $CO_2$ capture rate (91.7–100% *vs.* 93.8%). The relatively low hydrogen production cost achieved in all the plants of the study arises from the low cost of coal feedstocks and the benefits of the economies of scale provided by large hydrogen production capacities (13.3–15.7 € per GJ).

Hannula *et al.* 2021 (IEAGHG)[9] provided a techno-economic assessment of several biomass-to-X pathways, among which $BtH_2$ plants without and with CCS are studied. The plant without CCS includes oxygen-blown fluidized bed gasification, syngas reforming, two sour shift reactors, Rectisol-based $CO_2$ separation, PSA and a steam cycle. Compression of $CO_2$ is included when CCS is added, as separation of $CO_2$ is already present in the base case. A plant configuration where the $CO_2$ capture rate is maximised ($CCS_{max}$) is included in the analysis and it consists of capturing with MEA scrubbing the $CO_2$ contained in the flue gas produced by the combustion of the PSA tail gas and char in an auxiliary boiler. The plant with CCS reaches a $CO_2$ capture rate of about 90%. By adding MEA scrubbing, the capture rate is maximised up to 96.5%. The economic analysis is based on a first-of-a-kind (FOAK) plant assumption. The total capital investment of the biofuel demonstration plant GoBiGas is scaled up from 30 $MW_{LHV}$ to 103 $MW_{LHV}$ of biomass input. CCS components (*i.e.* $CO_2$ compression and post-combustion $CO_2$ capture) are added on top of the total capital investment. This analysis leads to a higher cost compared to other studies in the scientific literature. The integration of CCS starting from the base case costs about 20 € per $t_{CO_2}$. A cost of 92 € per $t_{CO_2}$ is required in order to maximise the $CO_2$ capture rate through the addition of MEA scrubbing.

In a carbon constrained economy with the objective of reaching net zero $CO_2$ emissions, biomass represents a scarce resource. Therefore, it is fundamental to make the best use of biogenic carbon according to market and societal needs and to sustainability criteria. The possible uses of biomass include its combustion to generate electricity and/or heat, and its conversion into a high value product (*e.g.* carbon-based products, bio-hydrogen, and biochar). As discussed in ref. 10 bio-energy plants integrated into the broader energy system may be required to cope with the intermittency of renewable energy sources (RES), that lead to variable prices of electricity on hourly time-scales and may lead to variable hydrogen prices on daily–monthly time scales depending on the cost of storage and on the flexibility of the market demand. Therefore, the expected time-dependent relative values of power, carbon-based products, hydrogen, and sequestered $CO_2$ may lead to economic benefits for plants integrated with electrolysis units increasing carbon utilization and product yield during low electricity price periods[11,12] and for multi-product plants operated flexibly to produce goods generating the highest revenues.

In this work, a techno-economic analysis of biomass-to-methanol and biomass-to-hydrogen plants with CCS is carried out, with the following main original outcomes:

(i) The calculation of the cost of $CO_2$ avoided for different products (methanol and hydrogen), different gasification technologies (direct oxygen-blown and indirect gasification) and different $CO_2$ capture strategies (pre-combustion MDEA-based and post-combustion MEA-based $CO_2$ capture);

(ii) The assessment of the economic impact of the design of plants with flexible production of methanol and hydrogen, when hydrogen is subject to time-dependent market prices.

## 2. Plant description

The following BECCS plants have been assessed in this work:

- The biomass-to-methanol plant, based on $O_2$-blown fluidized bed direct gasification (BtM DG);
- The biomass-to-methanol plant, based on dual fluidized bed indirect gasification (BtM IG);
- The biomass-to-hydrogen plant, based on $O_2$-blown fluidized bed direct gasification ($BtH_2$ DG);
- The biomass-to-hydrogen plant, based on dual fluidized bed indirect gasification ($BtH_2$ IG).

The block diagrams of the four assessed processes are shown in Fig. 1–4. All the plant configurations combine the same

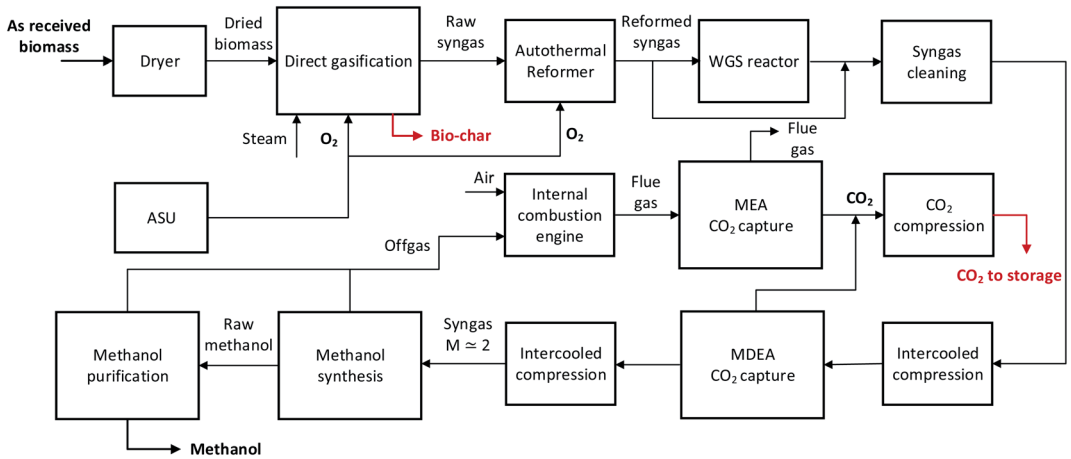


Fig. 1 Block diagram of the direct gasification-based biomass-to-methanol plant.

 

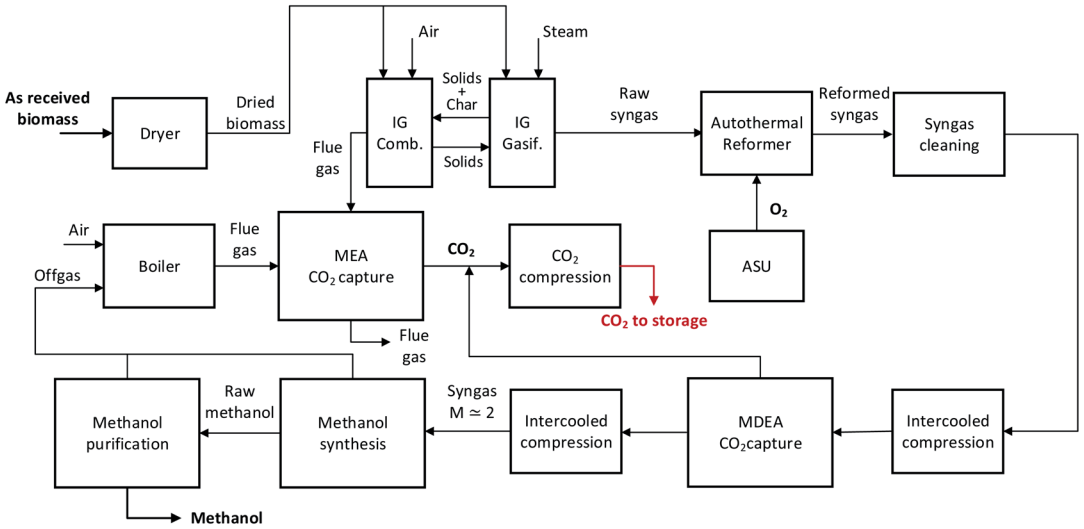


Fig. 2 Block diagram of the indirect gasification-based biomass-to-methanol plant.

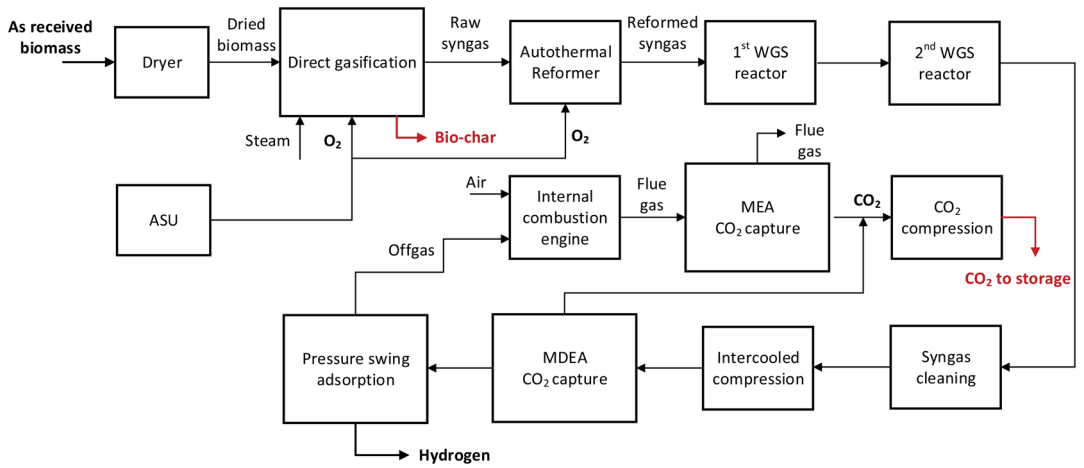


Fig. 3 Block diagram of the direct gasification-based biomass-to-hydrogen plant.

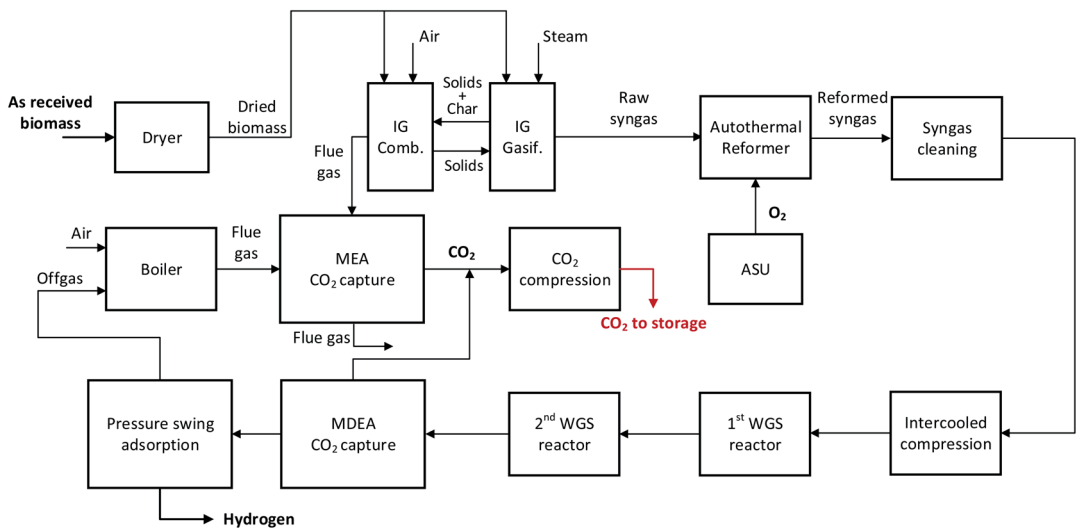


Fig. 4 Block diagram of the indirect gasification-based biomass-to-hydrogen plant.

Table 1 Summary of the selected recent literature on biomass-to-hydrogen plants. All the cost data are converted to 2019€. When not specified in the original paper, the currency year is assigned as: (year of publication − 1)

| Reference | Biomass input and gasification and syngas cleaning and conditioning technology | $CO_2$ capture efficiency | PSA $H_2$ recovery | Fuel efficiency | $CO_2$ capture rate | Main data for economic analysis | Cost of product |
|---|---|---|---|---|---|---|---|
| Larson *et al.* 2009[5] | Biomass input: 893 MW, 20% wt moisture. $O_2$-blown fluidized bed gasification, thermal/ catalytic cracking, two sour shift reactors, Rectisol, PSA, steam cycle. | ∼100% | 95% | 58.9% | — | Biomass cost: 4.0 € per GJ<br>TCI no CCS (per $kW_{prod}$)[a]: 1018 € per kW<br>TCI CCS (per $kW_{prod}$)[a]: - | No CCS: 13.6 € per GJ<br>CCS: - |
| Salkuyeh *et al.* 2018[6] | Biomass input: 1677 MW, 5.8% wt moisture. Indirect dual fluidized bed steam gasification, syngas reforming, high-T and low-T WGS reactors, MDEA, PSA, steam cycle (boiler fed with oxygen and additional natural gas –CCS– or with air -no CCS-). | N/A | N/A | 37.6% | 60% | Biomass cost: 4.6 € per GJ<br>TCI no CCS (per $kW_{prod}$): 982 € per kW<br>TCI CCS (per $kW_{prod}$): 1293 € per kW | No CCS: 24.7 € per GJ<br>CCS: 27.9 € per GJ<br>$CO_2$ avoidance marginal cost: 9.1 € per $t_{CO_2}$ |
| Salkuyeh *et al.* 2018[6] | Biomass input: 1327 MW, 5.8% wt moisture. Entrained flow $O_2$-blown gasification, high-T and low-T WGS reactors, MDEA, PSA, steam cycle (boiler fed with oxygen and additional natural gas –CCS– or with air -no CCS-). | N/A | N/A | 47.5% | ∼100% | Biomass cost: 4.6 € per GJ<br>TCI no CCS (per $kW_{prod}$): 1845 € per kW<br>TCI CCS (per $kW_{prod}$): 2033 € per kW | No CCS: 27.1 € per GJ<br>CCS: 27.9 € per GJ<br>$CO_2$ avoidance marginal cost: 6.6 € per $t_{CO_2}$ |
| Antonini *et al.* 2021[7] | Indirect dual fluidized bed steam gasification (heat pipe reformer), syngas reforming, high-T WGS reactor, MDEA (if CCS), PSA, steam cycle. | 98% | 90% | 58–65% | 60% | N/A | N/A |
| Antonini *et al.* 2021[7] | Sorption-enhanced $O_2$-blown gasification, syngas reforming, high-T WGS reactor, MDEA (if CCS), PSA, steam cycle. | 98% | 90% | 60–82% | 60% (oxy-comb) 92% (oxy-comb + MDEA) | N/A | N/A |
| Antonini *et al.* 2021[7] | Entrained flow $O_2$-blown gasification, high-T and low-T WGS reactors, MDEA (if CCS), PSA, steam cycle. | 98% | 90% | ∼55% | 98% | N/A | N/A |
| Del Pozo *et al.* 2021[8] | Coal & biomass input: 1255 MW, 30% wt biomass. Entrained flow $O_2$-blown gasification, two sour shift reactors, Selexol, PSA, steam cycle. | 95% | 90.5% | 59.3% | 93.8% | Biomass cost: 6.5 € per GJ<br>Coal cost: 2.7 € per GJ<br>TCI no CCS (per kWprod): -<br>TCI CCS (per kWprod): ∼1530 € per kW | No CCS: -<br>CCS[b]: 15.7 € per GJ |
| Del Pozo *et al.* 2021[8] | Coal & biomass input: 1255 MW, 30% wt biomass. Entrained flow $O_2$-blown gasification, high-T WGS reactor, membrane-assisted WGS. 1. Steam cycle. 2. More efficient gasification + gas turbine. 3. No power cycle (electricity import) + more steam to increase $H_2$ production. | — | — | 1. 62.9%,<br>2. 67.5%,<br>3. 73.0% | 1. ∼100%,<br>2. 91.7%,<br>3. ∼100% | Biomass cost: 6.5 € per GJ<br>Coal cost: 2.7 € per GJ<br>TCI no CCS (per $kW_{prod}$): -<br>TCI CCS (per $kW_{prod}$):<br>1. ∼1370 € per kW,<br>2. ∼1250 € per kW,<br>3. ∼1140 € per kW | No CCS: -<br>CCS[b]: 1. 14.3 € per GJ, 2. 13.8 € per GJ, 3. 13.3 € per GJ |

Table 1 (*Contd.*)

| Reference | Biomass input and gasification and syngas cleaning and conditioning technology | $CO_2$ capture efficiency | PSA $H_2$ recovery | Fuel efficiency | $CO_2$ capture rate | Main data for economic analysis | Cost of product |
|---|---|---|---|---|---|---|---|
| Hannula *et al.* 2021 (IEAGHG)[9] | Biomass input: 103 MW, 15% wt moisture. $O_2$-blown fluidized bed gasification, syngas reforming, two sour shift reactors, Rectisol, PSA, steam cycle, MEA (if $CCS_{max}$). | 97% (Rectisol) 90% (MEA) | 86% | 56.9% | 89.9% (Rectisol) 96.5% (Rectisol + MEA) | Biomass cost: 2.8 € per GJ TCI no CCS (per $kW_{prod}$): 6633 € per kW TCI CCS (per $kW_{prod}$): 6679 € per kW TCI $CCS_{max}$ (per $kW_{prod}$): 6847 € per kW | No CCS: 38.0 € per GJ CCS: 41.2 € per GJ $CO_2$ avoidance marginal cost: 20.3 € per $t_{CO_2}$ $CCS_{max}$: 42.2 € per GJ $CO_2$ avoidance marginal cost: 92.2 € per $t_{CO_2}$ |

[a] The overnight capital cost is reported. [b] $CO_2$ credit of 50 € per t is included.



fundamental conversion steps, namely biomass drying and gasification, syngas purification, conditioning and compression, final product synthesis and purification, and $CO_2$ removal and compression. All the plants are self-sufficient in terms of heat and steam balance, while grid electricity can be imported.

A description of the plant units and of the calculation methods is given in the next sections. Extensive tables with the properties of the main streams and the main calculation assumptions are reported in the ESI material (Table A1–A11).† Assumptions and calculation methods are consistent with our previous studies on power and biomass to methanol plants.[11,12]

The process models are developed using Aspen Plus®, which is used to compute the mass and energy balances of the integrated plants. The computations are conducted for a biomass input of 100 $MW_{LHV}$. The proximate and the ultimate analysis of the as-received woody biomass are assumed from the literature[13] and are reported in the ESI material.† Different thermodynamic models are considered for the different plant sections. The general model is the RKS-BM model that is complemented by the SRK model in the methanol synthesis section, the NRTL model in the methanol purification section, the ELECNRTL model in the water scrubber and the IAPWS-95 model for pure water streams.

### 2.1. Syngas production

The as-received woody biomass is fed to a belt dryer to reduce the moisture content from 45% to 15%, before feeding it to the gasification island. A detailed description of the belt drier can be found in the previous papers[11,12] and design specifications are reported in the ESI material (Table A11).†

In the direct gasification-based plants (Fig. 1 and 3), the gasifier is a pressurized circulating fluidized bed (CFB) which is fed with a mixture of steam and oxygen. Therefore, the gasification process is thermally sustained through the partial oxidation of biomass by means of oxygen from an air separation unit (ASU). Most of the inlet carbon remains in the nitrogen-free syngas as CO, $CO_2$ and $CH_4$, while a minor part is extracted from the fluidized bed as unconverted char.

In the indirect gasification-based plants (Fig. 2 and 4), the gasifier is a dual fluidized bed, constituted by a bubbling fluidized bed (BFB) gasifier and a circulating fluidized bed (CFB) combustor. A solid heat carrier material (*e.g.* olivine) circulates between the higher temperature combustor and the lower temperature gasifier to provide the heat required for biomass gasification. The heat is generated from the combustion with air of the unconverted char that flows from the gasifier to the combustor, and of additional biomass. A post-combustion $CO_2$ removal unit based on MEA scrubbing allows the capture of $CO_2$ from the flue gas generated in the combustor.

A detailed description of the model and of the design specifications of the gasification technologies can be found in ref. 12. The operating conditions are displayed in Table 2 and the comparison of the simulated syngas composition with literature data both for DG and IG is reported in the ESI material (Table A12).†

The aforementioned gasification processes generate a nitrogen-free syngas, which contains a significant amount of tar and methane. A catalytic auto-thermal reformer (ATR) unit is included downstream of the gasifier and a high temperature filtration unit, in order to convert methane and tar into CO and $H_2$. The ATR is fed with oxygen produced by an ASU with a purity of $95\%_{mol}$,[14] using catalysts designed to operate on raw syngas.[15] A restricted equilibrium calculation approach has been adopted for the ATR, assuming 90% methane conversion and complete conversion of higher hydrocarbons. Information about the operating conditions of the ATR for both the configurations is reported in Table 2.

The reformed syngas must be further conditioned, cleaned and compressed before the final product synthesis and purification. In all the configurations, a water scrubber allows the removal of soluble contaminants contained in the syngas, such as ammonia and chlorine. Bulk sulfur removal is performed

Table 2 Gasifiers and autothermal reformer operating conditions and exit gas composition

| Parameter | DG | IG |
|---|---|---|
| **Gasification** | | |
| Gasifier outlet temperature, °C | 870.0 | 815.0 |
| Gasifier outlet pressure, bar | 4.0 | 1.4 |
| $H_2$, $\%_{mol}$ dry, $N_2$, Ar free | 34.3 | 44.7 |
| CO, $\%_{mol}$ dry, $N_2$, Ar free | 25.0 | 23.1 |
| $CO_2$, $\%_{mol}$ dry, $N_2$, Ar free | 29.6 | 19.9 |
| $CH_4$, $\%_{mol}$ dry, $N_2$, Ar free | 7.6 | 9.7 |
| $C_xHy$, $\%_{mol}$ dry, $N_2$, Ar free | 3.4 | 2.6 |
| $H_2O$, $\%_{mol}$ | 40.2 | 36.3 |
| Syngas module at the gasifier outlet | 0.09 | 0.58 |
| Syngas flow rate, kmol $h^{-1}$ | 2058 | 1707 |
| Char conversion in the gasifier, % of inlet C | 95.50 | 83.00 |
| Biomass to gasifier, % of inlet biomass | 100.0 | 86.0 |
| Oxygen input, kg $s^{-1}$ | 1.93 | — |
| Carbon efficiency, % of inlet C | 95.50 | 71.39 |
| Fuel efficiency, $\%_{LHV}$ of dried biomass | 79.62 | 77.89 |
| Flow rate of solids from the combustor to the gasifier, kg $s^{-1}$ | — | 169.32 |
| **Syngas reforming** | | |
| Reformer outlet temperature, °C | 915.0 | 800.0 |
| Oxygen input, kmol $h^{-1}$ | 71.2 | 55.5 |
| $H_2$, $\%_{mol}$ dry, $N_2$, Ar free | 45.93 | 56.46 |
| $CO_2$, $\%_{mol}$ dry, $N_2$, Ar free | 24.28 | 17.87 |
| CO, $\%_{mol}$ dry, $N_2$, Ar free | 29.17 | 24.91 |
| S/C at the reformer inlet | 1.0 | 1.0 |
| Syngas module at the reformer exit | 0.41 | 0.90 |

using a liquid redox unit (LO-CAT process[16]), where $H_2S$ is converted into elemental sulfur and water by reaction with an iron oxygen carrier. The system is simulated as a black box, with data from ref. 17. An activated carbon bed and sulfur scavenging units, which are used to remove trace contaminants, are placed upstream of the last compression stage at a pressure of about 50 bar in methanol production plants, and upstream of the PSA at about 30 bar in hydrogen production plants.

### 2.2. Biomass-to-methanol plants

The methanol production plants must be fed with syngas with a module $M = (H_2 - CO_2)/(CO + CO_2)$ of around 2, which is achieved through syngas conditioning by means of a WGS reactor and/or $CO_2$ removal unit.

Downstream of the ATR in the DG-based plant, the syngas is cooled down to 220 °C and partly (about 27.4% of the total flow rate) fed to the adiabatic sour WGS reactor, which allows the adjustment of the syngas composition prior to the $CO_2$ removal step. The WGS inlet temperature is close to the lower end of the temperature range given by ref. 18 for raw gas shift (200–500 °C). A lower inlet temperature may also cause the condensation of residual tars.[19] It has to be remarked that conventional cobalt-molybdenum-based sour WGS catalysts require a minimum content of sulfur compounds in the dry raw gas of about 100–1500 ppm to maintain the catalyst activity.[18] With the biomass and the gasification conditions assumed in this study, the sulfur content in the sour WGS after direct gasification is around 100 ppm, meaning that the operating conditions should be validated with a catalyst vendor and the use or blending with higher sulfur biomass may be considered. In the IG-based plant, the WGS reactor is not present since the syngas composition does not require adjustments prior to $CO_2$ removal.

After bulk cleaning, syngas undergoes a compression to 30 bar through a 4-stage and a 6–stage intercooled compressor in DG- and IG-based plants, respectively. In all the configurations, the intercooler outlet temperature is 40 °C and the pressure ratio per stage $\beta_{stage}$ is about 1.8, leading to gas temperature at the outlet of each compression stage below 115 °C.

A pre-combustion $CO_2$ removal unit based on MDEA scrubbing at 30 bar allows the removal of the $CO_2$ contained in the syngas. In the DG-based plant, 95% of the $CO_2$ is separated from the syngas,[20] while in the IG-based plant, 90% of the $CO_2$ is removed to achieve the target module upstream of the methanol synthesis.

In BtM plants, a 2 stage intercooled compressor allows the pressure of the conditioned syngas to be increased to about 90 bar, which is the operating pressure of the methanol synthesis reactor. Downstream of the syngas purification, conditioning and compression steps, the fresh syngas with a module of 2.05 is fed to the methanol synthesis island.

The main features of the syngas conditioning process and the delivered syngas properties are summarized in Table 3.

The fresh syngas is first mixed with the unconverted recycled gas and then preheated in a feed/effluent heat exchanger, upstream of the methanol synthesis reactor. The stream from the methanol reactor is cooled down to 40 °C and separated in a flash unit from the light gases which are recycled back to the reactor.

 

Table 3 Main features of the syngas conditioning island

| Parameter | BtM DG | BtM IG | $BtH_2$ DG | $BtH_2$ IG |
|---|---|---|---|---|
| **Syngas conditioning** | | | | |
| WGS bypass, % | 72.56 | — | — | — |
| WGS reactor(s) inlet temperature, °C | 220 | — | 220/220 | 300/180 |
| Steam addition to the WGS reactor, kg $s^{-1}$ | — | — | — | 3.0 |
| $CO_2$ separation efficiency, % of inlet $CO_2$ | 95 | 90 | 95 | 95 |
| **Conditioned syngas properties** | | | | |
| Temperature, °C | 115.2 | 115.0 | 40.0 | 40.0 |
| Pressure, bar | 92.0 | 92.0 | 30.2 | 30.2 |
| Mass flow rate, kg $s^{-1}$ | 3.83 | 3.73 | 1.70 | 1.39 |
| Molar flow rate, kmol $h^{-1}$ | 1218 | 1214 | 1234 | 1218 |
| $H_2$, $\%_{mol}$ dry, $N_2$, Ar free | 67.33 | 67.32 | 93.41 | 94.77 |
| $CO_2$, $\%_{mol}$ dry, $N_2$, Ar free | 1.94 | 2.12 | 3.27 | 2.44 |
| CO, $\%_{mol}$ dry, $N_2$, Ar free | 29.96 | 29.69 | 2.56 | 1.93 |
| $CH_4$, $\%_{mol}$ dry, $N_2$, Ar free | 0.77 | 0.87 | 0.76 | 0.86 |
| $CO/CO_2$ | 15.44 | 14.02 | | |

Methanol synthesis is performed in a multi-tubular fixed bed reactor filled with commercial $Cu/ZnO/Al_2O_3$ catalyst (CZA) pellets and externally cooled by boiling water (*i.e.* boiling water reactor, BWR). The methanol synthesis is modeled using Aspen Plus as a plug flow reactor with the kinetic model proposed by Vanden Bussche *et al.*[21] Detailed information on the thermodynamics and the kinetics of the methanol reactor model can be found in ref. 22. The methanol synthesis reactor features a tube length of 6 m and diameter of 40 mm, a boiling water temperature of 238 °C and catalyst specifications as reported in Table A11 in the ESI material.† Moreover, the number of tubes in the reactor depends on the selected gas hourly space velocity (GHSV, defined as $Nm^3\ h^{-1}$ of reactor feed per $m^3$ of inner volume of reactor tubes). In this work, the plants are designed with a GHSV of 5000 $h^{-1}$ and a recycle ratio (RR, defined as the molar flow rate of the recycle stream divided by the molar flow rate of the fresh syngas) of 5.

The performance of the methanol synthesis unit is evaluated through the methanol carbon yield defined in eqn (2-1) and the methanol productivity (defined as the methanol produced per unit mass of the catalyst), where the produced methanol $F_{M,out}$ refers to the flow rate of liquid methanol downstream of the flash separator.

$$\text{Yield} = \frac{F_{M,\ out} - F_{M,\ in}}{(F_{CO_2} + F_{CO})_{in}} \quad (2\text{-}1)$$

The two methanol production plants have the same design specifications and a very similar $CO/CO_2$ ratio of the inlet syngas. As a consequence, the size and performance of the two systems are comparable (Table 4).

The raw product, rich in methanol and water with other trace species (low boiling components and ethanol), enters the purification section at 2 bar and about 40 °C, after throttling. Two distillation columns in series are employed; the first one removing most of the incondensable gases and the second one aimed at concentrating the methanol up to the desired purity of $99.85\%_{wt}$. Methanol recovery is at least $99.5\%_{mol}$ in both columns. The first column, *i.e.* the stabilizing column, accomplishes the separation with 20 trays, while the second one, *i.e.* the concentration column, performs the separation with 40 trays. The performance of the two plants is similar, as shown in Table 4.

The purge from the methanol synthesis and purification units contains a significant amount of light gases, whose heating value is exploited either in a cogenerative internal combustion engine (ICE) for electricity and steam production in the case of DG-based plants or in a boiler for steam production in the case of IG-based plants.

### 2.3. Biomass-to-hydrogen plants

The hydrogen production plants are designed with two WGS reactors with intercooling in order to increase the hydrogen fraction in the syngas. In the DG-based plant, two adiabatic sour WGS reactors are placed upstream of the compression step and operated at about 4 bar, similar to the gasifier. Both WGS reactors operate with an inlet temperature of 220 °C. The overall CO conversion in the WGS section is 93.1%. The first and second WGS reactors convert 75.5% and 71.9% of the inlet CO, respectively. In the IG-based configuration, the WGS section is placed downstream of syngas cleaning and compression and operates at about 30 bar. The first is a high-temperature WGS reactor with iron-based catalysts, fed with syngas at 300 °C, complying with the temperature range indicated by ref. 18 (300–510 °C). Upstream of the reactor, the syngas is mixed with superheated steam at 250 °C, with the flow rate tuned to reach a reduction factor $R = (p_{CO} + p_{H_2})/(p_{CO_2} + p_{H_2O})$ equal to 1.3, where $p_i$ is the partial pressure of the given species. Such a value is selected in order to avoid over-reduction of $Fe_3O_4$ in Fe-based high-temperature shift catalysts.[23] Since the syngas contains a very low amount of water at this step, a relatively high quantity of superheated steam (3.0 kg $s^{-1}$) must be added in order to reach the target value of the reduction factor. The second reactor is a low-temperature shift with copper-based catalysts. Syngas is fed at 180 °C, complying with the temperature range for low-temperature shift (180–270 °C).[18] The first and second

Table 4 Main features of the methanol synthesis and purification processes

| Parameters | BtM DG | BtM IG |
|---|---|---|
| **Methanol synthesis** | | |
| Number of tubes | 4345 | 4331 |
| GHSV, $h^{-1}$ | 5000 | 5000 |
| RR, molar basis | 5.0 | 5.0 |
| Recycle flow rate, kmol $h^{-1}$ | 6090 | 6071 |
| Methanol yield per pass, % | 63.74 | 69.33 |
| Overall methanol yield, % | 98.31 | 98.77 |
| Syngas module at the reactor inlet | 5.66 | 6.81 |
| Inert ($CH_4$, $N_2$, Ar) concentration at the reactor inlet, $\%_{mol}$ | 44.90 | 40.15 |
| Syngas temperature at reactor inlet, °C | 187.4 | 186.35 |
| Thermal power released by the reactor, MW | 6.95 | 6.86 |
| Methanol concentration at the reactor outlet, $\%_{mol}$ | 6.22 | 6.29 |
| Methanol concentration at the flash unit outlet, $\%_{mol}$ | 93.07 | 92.54 |
| Methanol productivity, kg $day^{-1}$ $kg_{cat}^{-1}$ | 13.03 | 13.21 |
| **Methanol purification** | | |
| Inlet mass flow rate, kg $s^{-1}$ | 3.46 | 3.50 |
| Inlet molar flow rate, kmol $h^{-1}$ | 398 | 405 |
| Inlet methanol concentration, $\%_{mol}$ | 93.07 | 92.54 |
| Inlet $H_2O$ concentration, $\%_{mol}$ | 4.77 | 5.51 |
| **Stabilizing column** | | |
| Condenser duty, MW | 0.013 | 0.012 |
| Reflux ratio | 0.11 | 0.11 |
| Reboiler duty, MW | 0.84 | 0.85 |
| **Concentration column** | | |
| Condenser duty, MW | 5.84 | 5.97 |
| Reflux ratio | 0.63 | 0.64 |
| Reboiler duty, MW | 5.68 | 5.81 |

WGS reactors convert 63.4% and 82.2% of the inlet CO, respectively, leading to an overall CO conversion of 93.5%.

Syngas compression to 30 bar is carried out through a 4-stage and a 6-stage intercooled compressor, respectively in DG- and IG-based plants. In all the configurations, the intercooler outlet temperature is 40 °C and the pressure ratio per stage $\beta_{stage}$ is about 1.8, leading to gas temperature at the outlet of each compression stage below 115 °C.

In both DG- and IG-based plants, a pre-combustion $CO_2$ removal unit based on MDEA scrubbing at 30 bar allows the removal of 95% of the $CO_2$ contained in the syngas.

Downstream of $CO_2$ removal, $H_2$-rich syngas at 30 bar is fed to the PSA unit without additional compression. The syngas specifications for the plant configurations are shown in Table 3. The products of the PSA system are hydrogen with a purity of higher than $99.99\%_{vol}$ at 30 bar and a tail gas stream at atmospheric pressure. The hydrogen separation efficiency of the PSA is assumed to be 90%.[24]

The heating value of the light gases in the PSA tail gas is exploited either in a cogenerative internal combustion engine (ICE) for electricity and steam production in the DG-based plant or in a boiler for steam production in the IG-based plant, as discussed in Section 2.5.

### 2.4. $CO_2$ capture

The studied plants are designed to capture the $CO_2$ produced during the conversion of biomass into the final product. As a consequence, the carbon which is captured from the air during the biomass growth can be stored underground resulting in a negative emission process.

The technologies considered in this work for $CO_2$ separation are pre-combustion and post-combustion chemical absorption processes based on MDEA and MEA solvents respectively. In methanol production plants, $CO_2$ is removed by means of MDEA scrubbing in order to reach the target module necessary for the downstream synthesis. In hydrogen production plants, $CO_2$ is removed from the syngas in order to obtain a high-purity $CO_2$ stream. The post-combustion technology may be employed in all the plant configurations in order to increase the overall $CO_2$ capture rate. The IG-based plants adopt MEA scrubbing to separate the $CO_2$ from the flue gases coming from both the CFB combustor and from the PSA tail gas boiler. The DG-based plant uses post-combustion technology in order to separate the $CO_2$ from the flue gas of the ICE which burns the off-gas of the methanol synthesis and purification. The amount of high-purity $CO_2$ coming from the amine scrubbing units changes significantly according to the gasification technology and the product. As shown in the ESI material (Table A1–A10),† the mass flow rate of separated $CO_2$ with MDEA ranges between 2.79 kg $s^{-1}$ of the BtM IG case, where most of the carbon is retained in the

 

product and released as $CO_2$ from the combustor, and 9.09 kg $s^{-1}$ of the $BtH_2$ DG case, where most of the carbon has to be separated as $CO_2$ from the syngas. The mass flow rate of separated $CO_2$ with MEA is 0.20 and 0.92 kg $s^{-1}$ for BtM DG and $BtH_2$ DG respectively. For IG-based plants, 2.88 kg $s^{-1}$ is separated from the flue gas of the CFB combustor and 0.19 and 0.73 kg $s^{-1}$ from the flue gas of the boiler for BtM IG and $BtH_2$ IG respectively.

As the selected amine scrubbing processes are well-known commercial technologies, the $CO_2$ removal units are not modelled in detail, but the amount of $CO_2$ to be separated is set to 90–95%, as mentioned in Sections 2.2 and 2.3. The reboiler duty of the stripping column is set to 1 MJ $kg_{CO_2}^{-1}$ for MDEA[25–27] and 3.7 MJ $kg_{CO_2}^{-1}$ for MEA scrubbing.[28] The electricity consumption of the two technologies, that has a little impact on the overall electricity balance, is derived from ref. 29. $CO_2$ is assumed to be released from the stripping columns with 100% purity (dry basis) at near atmospheric pressure.

Once separated in the respective amine scrubbing units, the captured $CO_2$ stream is sent to the compression unit, composed of an intercooled compressor followed by a pump. The 5-stage intercooled compressor pressurizes the $CO_2$ up to 80 bar with a pressure ratio per stage of about 2.3 and an intercooler outlet temperature of 40 °C. Downstream of the last compressor, supercritical $CO_2$ is pumped up to 150 bar. The overall electricity consumption of the compression process is 0.11 kW $h_{el}$ $kg_{CO_2}^{-1}$, which is consistent with the literature.[19]

### 2.5. Thermal integration

Biomass-to-X plants make available significant amounts of heat to be recovered from many sources (*e.g.* hot syngas, flue gas, methanol synthesis, *etc.*). However, a great amount of the recovered heat is needed to provide heat for amine regeneration, for methanol purification, and to generate steam for the gasification unit. This can be partly supplied by the combustion of the tail gas from the methanol synthesis process and from the PSA for hydrogen purification. Such off-gases are exploited either in a cogenerative ICE for electricity and steam production (in DG-based plants), or in a boiler for steam production (in IG-based plants). IG-based plants face a higher heat demand compared to DG-based plants due to the larger capacity of the post-combustion $CO_2$ separation process, which is more energy intensive. In the DG-based plants, the energy balance of the ICE is evaluated by using linearized equations derived from ref. 30. Such equations allow computation of the electric power, the net electric efficiency, the thermal power and thermal efficiency of the ICE. ICEs feature an electric efficiency of between 44.7 and 46.4% and a thermal efficiency of between 44.4 and 45.6%. The flue gases exit the ICE at 400 °C and are cooled down to 100 °C by recovering 18.6–19.8% of the fuel energy input. The rest of the heat is transferred to the cooling circuit of the ICE and can be recovered at low temperature, if required. In the IG-based plants, the high temperature flue gases from the boiler are first cooled down to 160 °C by steam generation and then to 80 °C for combustion air pre-heating.

In Table 5, the heat available and the thermal loads are shown for each plant configuration. The available high temperature heat is much higher in the IG-based plants compared to the DG cases. This is due to the high temperature flue gas from the CFB combustor and to the tail gas boiler. The methanol production plants require boiling water for the cooling of the reactor, which is not present in the hydrogen production plants. The availability of low temperature heat is similar among the BECCS plants. The methanol production plants can exploit a considerable amount of thermal power from the methanol cooler upstream of the flash unit and the purification section. The hydrogen production plants have higher heat recovery potential in the $CO_2$ compression section due to the higher $CO_2$ mass flow rate. The DG-based plants can exploit the heat recovery from the cooling circuit of the ICE.

As previously mentioned, the IG-based plants require larger amounts of heat due to the higher amount of $CO_2$ separated with the post-combustion capture technology. The BtM DG-based plant has a similar thermal consumption to the $BtH_2$ DG configuration because the heat required by the reboiler of the methanol concentration column balances the higher heat requirement of the $CO_2$ removal units which handle a higher mass flow rate to be separated. The same happens with the IG-based plants which share a similar amount of high temperature heat consumption. The low temperature heat demand is the same for all the configurations and is related to the hot water requirement of the belt dryer. Steam generation is required for the gasification unit mainly for fluidizing the bed and for sealing and cleaning purposes. In $BtH_2$ IG, superheated steam is required for the high temperature WGS reactor in order to avoid catalyst over-reduction, as described in Section 2.3.

The thermal integration for all the configurations depends on the heat available and the thermal loads within the plant. In none of the biomass-to-X plants, heat is recovered with a steam cycle as the high heat demand for $CO_2$ removal does not leave heat available for power generation or does not make it economically competitive to produce very small electric power output. Furthermore, the technical constraint related to the metal dusting,[31] which forbids superheating the steam with the syngas cooler, involves low superheating temperature and low steam cycle efficiency. Therefore, steam/water loops are adopted in all the configurations to transfer heat from waste heat sources to the heat users. The TQ diagrams of the four plants are reported in Fig. A5–A8 (ESI material).†

In the BtM DG plant, as shown in the temperature heat diagram in Fig. A5,† two water loops at different evaporation pressures are adopted. In the high pressure loop, the evaporation pressure (32.2 bar) is fixed by the methanol reactor. The saturated steam from the BWR is condensed back to provide heat to the distillation column reboilers. The evaporation pressure of the low pressure loop is 6 bar. In the syngas cooler upstream of the sour WGS reactor, steam is evaporated. Part of it is slightly superheated to 200 °C and fed to the gasifier and the remaining part is supplied to the MDEA and MEA reboilers.

Similarly to the previous configuration, the BtM IG plant (Fig. A6†) adopts two water loops for heat recovery. As in the previous case, the high pressure loop at 32.2 bar is fixed by

Table 5 Heat availability and thermal loads of the assessed plants

| Thermal loads | BtM DG | BtM IG | $BtH_2$ DG | $BtH_2$ IG |
|---|---|---|---|---|
| *High-medium temperature heat available (suitable for steam generation, amine regeneration, and methanol purification), $MW_{th}$* | *24.24* | *32.46* | *21.20* | *35.95* |
| Flue gas cooler | — | 9.64 | — | 9.64 |
| Syngas cooler 1 | 16.80 | 11.27 | 16.79 | 11.27 |
| Syngas cooler 2[a] | — | — | 3.73 | — |
| Clean syngas cooler 1 | — | — | — | 1.90 |
| Clean syngas cooler 2[b] | — | — | — | 1.67 |
| Methanol synthesis | 6.95 | 6.86 | — | — |
| ICE flue gas | 0.49 | — | 0.68 | — |
| Tail gas boiler | — | 4.69 | — | 11.47 |
| *Low temperature heat available (suitable for biomass drying), $MW_{th}$* | *16.92* | *17.08* | *14.33* | *15.14* |
| Syngas compressor intercoolers 1 | 4.25 | 5.78 | 5.33 | 5.02 |
| Syngas compressor intercoolers 2[c] | 0.78 | 0.77 | — | — |
| Clean syngas cooler 3 | — | — | — | 5.59 |
| Methanol cooler | 7.75 | 7.98 | — | — |
| $CO_2$ compressor intercoolers | 2.41 | 2.55 | 4.36 | 4.53 |
| ICE low temperature water cooler | 1.73 | — | 4.64 | — |
| *Medium temperature heat demand, $MW_{th}$* | *12.58* | *20.83* | *12.49* | *20.14* |
| Stabilizing column reboiler, $MW_{th}$ | 0.84 | 0.85 | — | — |
| Concentration column reboiler, $MW_{th}$ | 5.68 | 5.81 | — | — |
| Pre-combustion $CO_2$ capture (MDEA), $MW_{th}$ | 5.32 | 2.79 | 9.09 | 6.78 |
| Post-combustion $CO_2$ capture (MEA) (comb. Fraction), $MW_{th}$ | — | 10.66 | — | 10.67 |
| Post-combustion $CO_2$ capture (MEA) (ICE/boiler fraction), $MW_{th}$ | 0.74 | 0.72 | 3.40 | 2.69 |
| *Low temperature heat demand (for biomass drying), $MW_{th}$* | *13.04* | *13.04* | *13.04* | *13.04* |
| Steam generation, $\dot{m}$ [kg $s^{-1}$]/$T$ [°C]/$p$ [bar] | 2.66/200/6[d]<br>0.80/200/6 | 2.62/400/4[d]<br>0.69/180/4 | 2.66/200/6[d]<br>0.80/200/6 | 2.62/400/4[d]<br>0.69/180/4<br>3.00/250/33 |

[a] Syngas cooler 2 is placed in between the sour WGS reactors. Syngas cooler 1 is the heat exchanger immediately downstream of the gasification and reforming section. [b] Clean syngas cooler 2 is placed downstream of the low-temperature WGS reactor. Clean syngas cooler 1 is in between high-temperature and low temperature WGS reactors. [c] Syngas compressor intercoolers 2 correspond to the compressor which performs compression prior to methanol synthesis (up to 90 bar). [d] The first row corresponds to the gasifier fluidization steam. The second row includes steam for sealing and cleaning purposes in the gasification section. The third row is the steam addition to the high-temperature WGS in $BtH_2$ IG.

methanol reactor cooling. Saturated steam is sent to the distillation column reboilers. In the low pressure loop, the evaporation takes place at 4 bar with part of the cooling of the flue gas from the CFB combustor, the syngas cooling upstream of the water scrubber and the flue gas cooler downstream of the boiler. Part of the saturated steam is preheated to 400 °C (fluidizing steam) and to 180 °C (steam for cleaning and sealing purposes) through the heat provided by the flue gas from the CFB combustor. The remaining part of the produced steam supplies heat to the MDEA and MEA reboilers.

The $BtH_2$ DG plant (Fig. A7†) has one low pressure water loop at 6 bar. The evaporation is carried out in the syngas cooling section and with part of the flue gas cooler downstream the ICE. The saturated steam is partly superheated to 200 °C and sent to the gasifier. The remaining steam provides heat for the regeneration of MDEA and MEA.

 

The $BtH_2$ IG plant (Fig. A8†) adopts two water evaporation levels. The high pressure level is needed to provide steam to the WGS reactors. Steam is evaporated at 33 bar and slightly superheated to 250 °C in the syngas cooler upstream of the water scrubber. The low pressure loop operates at 4 bar. The heat sources exploited for steam evaporation are the hot syngas upstream of the water scrubber, the flue gas from the CFB combustor and from the tail gas boiler, and the hot syngas downstream of the high-temperature and the low-temperature WGS. Part of the saturated steam is preheated to 400 °C (fluidizing steam) and to 180 °C (steam for cleaning and sealing) through the heat provided by the flue gas from the CFB combustor. The remaining part of the steam supplies heat to the MDEA and MEA reboilers. A make-up is provided to balance out the process steam consumed in the gasifier and the WGS unit.

In all the configurations, low temperature heat is used to provide the heat needed in the belt drier (see Table 7). A water loop from 90 to 30 °C supplies about 13 $MW_{th}$ for biomass drying.

### 2.6. Flexible methanol and hydrogen production

Methanol price varies over time, depending on the global market. Even though hydrogen is not currently traded as a commodity, this may change in the future, when increasing amounts of green hydrogen may be produced from renewables and its availability and price may change on a seasonal basis. In such a context, multi-product plants may take economic advantage by operating flexibly to produce the good (methanol or hydrogen in this case) that generates the highest revenues. In order to design a plant which flexibly produces methanol and hydrogen, all the components must be designed to operate under both the operating conditions, *i.e.* methanol production mode and hydrogen production mode.

In both biomass-to-methanol & hydrogen plants based on direct gasification ($BtMH_2$ DG) and on indirect gasification ($BtMH_2$ IG), the gasification island is designed and operated stably, since its operation is independent of the operating mode. On the other hand, the process units downstream of the gasifier and the reformer can be designed for methanol or hydrogen operation mode and may be bypassed depending on the operating point.

In the DG-based plant, two sour WGS reactors are present for the production of hydrogen. In methanol production mode, WGS reactors should be partly or totally bypassed. Downstream of the scrubber all the plant components are designed for the hydrogen production case due to the higher flow rate in this configuration (more syngas shift and therefore less water removed in the scrubber purge). The methanol synthesis and purification islands (including the 2nd syngas compressor) and the hydrogen production island are both installed to provide the different products according to the market needs. The $CO_2$ capture and compression units are designed for the hydrogen production case, since a higher $CO_2$ flow rate is separated in hydrogen production mode. The high pressure steam generation loop is dedicated to the methanol production (methanol synthesis reactor and distillation columns). The low pressure loop is present in both the configurations and it is designed in the hydrogen production mode.

In the IG-based plant, the methanol and hydrogen production plants are identical up to the syngas compressor (same flow rates, pressures and temperatures of the streams). Downstream of the compression stage, the hydrogen production mode needs a high temperature WGS reactor and a low temperature WGS reactor in order to maximize the hydrogen production. In the methanol production mode, WGS reactors should be partly or totally bypassed. As in the previous case, methanol and hydrogen production islands are both installed and the units for $CO_2$ capture are designed in the hydrogen production mode. A high pressure steam generation loop is dedicated to methanol production (methanol synthesis reactor and distillation columns). Another high pressure level is necessary to provide the steam requirement for the WGS in the hydrogen case. In this case, the syngas cooler and the flue gas cooler provide heat both to the high pressure and the low pressure levels.

## 3. Process simulation results

In order to assess the performance of the BECCS plants described in this work, the following key performance indicators have been selected.

The fuel efficiency ($\eta_{F,i}$) is the ratio between the chemical energy of the product stream and the chemical energy input to the process (both based on LHV). The fuel efficiency can be evaluated for the whole plant or for any plant process unit (i).

$$\eta_{F,i} = \frac{\dot{m}_{out,\,i} \cdot LHV_{out,i}}{\dot{m}_{in,i} \cdot LHV_{in,i}} \tag{3-1}$$

The carbon efficiency ($CE_i$) can be defined as the ratio between the carbon molar flow rate in the stream $F_{C,i}$ at the exit of each process unit i and the carbon molar flow rate in the inlet biomass stream $F_{C,biom}$.

$$CE_i = \frac{F_{C,i}}{F_{C,biom}} \tag{3-2}$$

The equivalent fuel efficiency ($\eta_{F,eq}$) accounts for the biomass saving associated with the electricity production of the plant. A steam cycle with 35% electric efficiency ($\eta_{el,ref}$) is assumed as a reference, considering a biomass-fed subcritical steam power plant.

$$\eta_{F,eq} = \frac{\dot{m}_M \cdot LHV_M}{\dot{m}_{biom} \cdot LHV_{biom} - \frac{P_{el}}{\eta_{el,ref}}} \tag{3-3}$$

The carbon capture rate (CCR) is the percentage of stored carbon with respect to the carbon contained in the feedstock

$$CCR = \frac{F_{C,stored}}{F_{C,biom}} \tag{3-4}$$

Table 6 Overall performance of the assessed plants

| Performance indexes | BtM DG | BtM IG | $BtH_2$ DG | $BtH_2$ IG |
|---|---|---|---|---|
| $\eta_{F,\mathrm{dryer}}$, % | 108.75 | 108.75 | 108.75 | 108.75 |
| $\eta_{F,\mathrm{gas}}$, % | 79.62 | 77.89 | 79.62 | 77.89 |
| $\eta_{F,\mathrm{ref}}$, % | 97.47 | 99.26 | 97.47 | 99.26 |
| $\eta_{F,\mathrm{pur\text{-}co}}$, % | 98.70 | 99.97 | 94.33 | 95.46 |
| $\eta_{F,\mathrm{syn}}$, % | 79.48 | 79.83 | — | — |
| $\eta_{F,\mathrm{f\_pur}}$, % | 98.27 | 98.03 | 84.97 | 85.38 |
| **$\eta_{F,\mathrm{global}}$, %** | **65.07** | **65.77** | **67.65** | **68.53** |
| **$\eta_{F,\mathrm{eq}}$, %** | **50.35** | **48.29** | **55.36** | **50.15** |
| **Carbon efficiency, %** | **42.34** | **42.81** | — | — |
| **Carbon capture rate, %** | **56.60** | **55.34** | **98.98** | **98.14** |
| Oxygen demand, kg $s^{-1}$ | 2.57 | 0.50 | 2.57 | 0.50 |
| Biofuel production, kg $s^{-1}$ | 3.27 | 3.31 | 0.56 | 0.57 |
| Biofuel output, $MW_{LHV}$ | 65.07 | 65.77 | 67.65 | 68.53 |
| Net electric output, $P_{el}$, MW | −9.93 | −12.31 | −7.55 | −12.46 |
| Electricity generation, MW | 2.17 | — | 5.55 | — |
| Electricity consumption, MW | 12.10 | 12.31 | 13.10 | 12.46 |
| Belt dryer electricity consumption | 0.65 | 0.65 | 0.65 | 0.65 |
| Gasification combustor air fan | — | 0.68 | — | 0.68 |
| Gasification oxygen compressor | 0.24 | — | 0.24 | — |
| Syngas compressor 1 | 4.49 | 5.77 | 5.58 | 5.98 |
| Syngas compressor 2 | 1.66 | 1.66 | — | — |
| Methanol loop recycle compressor | 0.38 | 0.38 | — | — |
| MDEA electricity consumption | 0.23 | 0.12 | 0.40 | 0.30 |
| MEA electricity consumption | 0.02 | 0.28 | 0.08 | 0.32 |
| ASU[a] | 2.27 | 0.49 | 2.27 | 0.49 |
| $CO_2$ compression | 2.13 | 2.25 | 3.85 | 4.00 |
| Other auxiliaries[b] | 0.03 | 0.03 | 0.03 | 0.04 |
| Total waste water, kg $s^{-1}$ | 3.84 | 3.71 | 2.52 | 5.35 |
| Water make-up, kg $s^{-1}$ | 3.46 | 3.30 | 3.46 | 6.30 |
| Net water consumption, kg $s^{-1}$ | −0.38 | −0.41 | 0.94 | 0.95 |

[a] Specific consumption depending on size from ref. 32. [b] Other auxiliaries include liquid redox, water scrubber pumps and water loop pumps.

The described performance indices alongside other significant quantities are reported in Table 6.

The DG-based plants show the highest gasifier fuel efficiency ($\eta_{F,\mathrm{gas}}$) which is mainly due to the use of oxygen as an oxidant instead of air. The benefits of oxygen-blown gasification counterbalance the overall lower char conversion in the gasification system and the feed of steam at lower temperature. The lower fuel efficiency of the reformer ($\eta_{F,\mathrm{ref}}$) in the DG configurations with respect to the IG cases is due to the higher syngas flow rate and to the higher difference between the gasifier and reformer exit temperatures, that cause a higher oxygen demand to heat up the raw syngas to the reforming temperature. The loss of fuel efficiency in the purification and conditioning step ($\eta_{F,\mathrm{pur\text{-}co}}$) is due to the exothermicity of the WGS reaction. The higher efficiency loss of the hydrogen production plants is due to the greater advancement of the WGS reaction. With regard to the fuel efficiencies of the synthesis ($\eta_{F,\mathrm{syn}}$) and of the purification sections ($\eta_{F,\mathrm{f\_pur}}$) in the methanol production plants, the differences among the cases are modest and mainly related to the differences in the $CO/CO_2$ ratio of the syngas. The loss of efficiency in the methanol synthesis is due to both the exothermicity of the reaction and the tail gas extraction. In both plants, almost 80% of the fresh syngas thermal power ends up in crude methanol, about 5% is released with the tail gas and about 15% is lost with the exothermic reaction. The loss of efficiency in the last step of the hydrogen production plants is due to the loss of hydrogen and other fuel gases (*e.g.* $CH_4$, CO) as tail gas from the PSA unit. The resulting overall fuel efficiencies are slightly higher in the hydrogen plants (67.6–68.5%) than in the methanol plants (65.1–65.8%). The bio-hydrogen plant studied by Hannula *et al.*,[9] which shares a similar plant configuration to the $BtH_2$ DG plant assessed in this work, features a global fuel efficiency of 56.9% referred to the biomass LHV downstream of the dryer (*vs.* 62.2% of $BtH_2$ DG referred to dried biomass). The difference is mainly due to the higher hydrogen separation efficiency in the PSA of the $BtH_2$ DG plant assumed in this work (90% *vs.* 86%). Overall, the aforementioned fuel efficiencies obtained in this work are in the high range of the interval of values reported for similar plants in the literature (see Table 1).

The carbon efficiencies show modest differences in methanol production plants, ranging from 42.3 to 42.8%.

The electricity consumption of the investigated plants does not show substantial differences, as all plants need to import between 12.1 and 13.1 $MW_e$. In all plants, most of the electricity consumption is associated with syngas compression, followed by $CO_2$ compression and $O_2$ production (in DG-based plants). The hydrogen production plants show higher $CO_2$ compression

 

Table 7 Carbon balance of the BECCS plants. Percent values refer to the total inlet carbon

| | *C* in fuel | Captured $CO_2$ (MDEA) | Captured $CO_2$ (MEA, from gasification unit) | Captured $CO_2$ (MEA, from vented gas combustion in ICE/ boiler) | Bio-char | Vented $CO_2$ |
|---|---|---|---|---|---|---|
| BtM DG | 42.3% | 50.3% | — | 1.9% | 4.5% | 1.1% |
| BtM IG | 42.8% | 26.3% | 27.2% | 1.8% | — | 1.9% |
| $BtH_2$ DG | — | 85.8% | — | 8.7% | 4.5% | 1.0% |
| $BtH_2$ IG | — | 64.0% | 27.2% | 6.9% | — | 1.9% |

power, since a higher portion of the inlet carbon is separated as $CO_2$. The DG-based plants feature higher ASU consumption due to higher oxygen demand. In the DG-based plants, the electricity consumption is partly compensated by the electricity production of the ICE. This is not the case of the IG-based plants, where tail gas is burned in boilers rather than in the ICE, due to the higher heat demand for $CO_2$ separation.

The steam produced within the plants partly allows the heat demand of the thermal loads to be satisfied and is partly consumed in the gasifier and in the high-temperature WGS reactor (only in $BtH_2$ IG). In DG-based plants, a higher amount of water is injected into the gasifier to reach the target steam-to-carbon ratio upstream of the reformer, since a higher amount of carbon is retained in the syngas. As a consequence, considering only the contribution to the gasifier, a higher amount of water make-up is required in DG-based plants. However, in $BtH_2$ IG, superheated steam is added before the high-temperature shift reactor to avoid catalyst over-reduction.

The injected steam is partly converted into hydrogen through gasification, reforming and/or WGS and partly condensed back to liquid water. Most of the condensed water comes from the water scrubber purge. From 8 to 27% of the total waste water derives from flue gas cooling, before MEA-based $CO_2$ absorption. The waste water can be recovered and re-used within the plant after treatment. Methanol production plants do not require a net water addition, while hydrogen production plants need a net addition. This is related to the fact that in hydrogen production plants more syngas is shifted and therefore more water is converted into hydrogen.

Table 7 shows the fate of carbon in the assessed plants. The biogenic carbon which is contained in the biomass can be retained in the final product (in the case of methanol production), captured and stored, and vented as $CO_2$. Most of the carbon is captured through pre- and post-combustion $CO_2$ technologies. In the direct gasifier, a small quantity of bio-char is also released with the fluidized bed solids purge. In all the plant configurations, less than 2% of the biogenic carbon is vented to the atmosphere as $CO_2$. In DG-based plants, most of the $CO_2$ is captured by the pre-combustion MDEA process (50% and 86% in the case of methanol and hydrogen production, respectively) and a much lower amount of $CO_2$ is captured post-combustion with MEA (2% and 9% for methanol and hydrogen production, respectively). In contrast, in IG-based plants, post-combustion capture is necessary to achieve high $CO_2$ capture efficiency, as 27% of the total inlet carbon is captured from the IG combustor. On the whole, $CO_2$ vented to the atmosphere is about 1% of the inlet carbon in the DG-based plants and 2% in the IG based-plants.

It is important to note that this analysis does not include the impact of indirect $CO_2$ emissions from the biomass supply chain and from imported electricity. In this respect, considering that the assessed plants consume between 0.40 and 0.66 MWh of electricity per ton of carbon in the inlet biomass, indirect emissions from power consumption would correspond to 1.0–1.6% of the biogenic carbon fed to the plant if derived from 50 $kg_{CO_2}$ $MWh^{-1}$ electricity, or to 5.9–9.8% of the biogenic carbon fed to the plant if derived from 300 $kg_{CO_2}$ $MWh^{-1}$ electricity.

# 4. Economic analysis

The economic analysis is performed by using the levelized cost approach. The levelized cost of fuel (LCOF) is defined as the breakeven selling price of the produced product ($M_{tot}$) that repays the total costs ($C_{tot}$) at the end of the plant lifetime (LT). The LCOF depends on the total capital investment (TCI) costs, the utilities costs ($C_{ut}$), the cost of the feedstock ($C_{feedstock}$) and the fixed O&M costs ($C_{fixed\ O\&M}$), as shown in eqn (4-1), where $\dot{m}_{fuel}$ is the nominal fuel production rate and $h_{eq}$ represents the equivalent yearly operating hours. Consistent with all the literature on techno-economic studies on biomass conversion *via* gasification, a high capacity factor (90%) has been assumed,

Table 8 Main assumptions and parameters for the economic analysis

| Economic parameters | Value |
|---|---|
| Discount rate, % | 10.0 |
| Lifetime, *y* | 20 |
| Capital charge factor, % | 11.75 |
| Annual availability, h $year^{-1}$ | 7884 |
| **Variable opex** | |
| Biomass feedstock cost, € per t | 45.72 |
| 2019 Denmark average electricity price, € per MWh | 38.49 |
| $CO_2$ transport and injection/storage costs, € per t | 13.39 |
| **Fixed opex** | |
| Maintenance and repairs, % FCI | 5 |
| Operating supplies, % FCI | 0.5 |
| Operating labor, % opex | 10 |
| Laboratory costs, % opex | 2.5 |
| Local taxes, % FCI | 1 |
| Insurance, % FCI | 1 |
| Methanol synthesis catalyst cost, € per kg | 18.12 |
| Catalyst lifetime, *y* | 4 |

which is needed to make high capex processes economically competitive.

$$\mathrm{LCOF} = \frac{C_{\mathrm{tot}}}{M_{\mathrm{tot}}} = \frac{\mathrm{TCI}\cdot\mathrm{CCF} + C_{\mathrm{fixed\ O\&M}} + C_{\mathrm{feedstock}} + C_{\mathrm{ut}}}{\dot{m}_{\mathrm{fuel}}\cdot h_{\mathrm{eq}}} \quad (4\text{-}1)$$

The method for capex and opex estimation is extensively described in previous articles.[11,12] The main assumptions, coherent with our previous studies, are summarized in Table 8. All the costs reported in this paper refer to the year 2019. The details of the capital costs of the plant equipment are reported in the ESI material (Table B3–B7).† The $CO_2$ transport and injection/storage costs are considered to be equal to 13.4 € per t. The assumed cost corresponds to a 100 km pipeline transport from the conversion facility to the storage site and 2 km underground storage in deep saline formations.[9]

The details of the fixed capital investment (FCI) costs of the BECCS plants are shown in Table 9. The FCI is derived by subtracting the working capital from the total capital investment (see Table B1 in ESI information†). Alongside the BtM and $BtH_2$ plants, the flexible plants (*i.e.* $BtMH_2$ DG and $BtMH_2$ IG) described in Section 2.6, are included in the table. The biomass-to-syngas island cost differs depending on the gasification technology. However, the cost of the DG- and IG-based plants is similar, as the higher cost of the ASU in the DG-based plants is offset by the higher cost of the dual fluidized bed gasification. The methanol production plants hold the lowest syngas purification, conditioning and compression costs, since they do not have or have a smaller WGS section. The flexible methanol and hydrogen production plants have the highest syngas purification, conditioning and compression costs, since they require both the higher cost WGS section for hydrogen production, and

Table 9 Breakdown of the fixed capital investment costs of the biomass to methanol (BtM), biomass to hydrogen ($BtH_2$) and flexible biomass to methanol and hydrogen ($BtMH_2$) plants

| Fixed capital investment | BtM DG | BtM IG | $BtH_2$ DG | $BtH_2$ IG | $BtMH_2$ DG | $BtMH_2$ IG |
|---|---|---|---|---|---|---|
| **Biomass-to-syngas, M€** | **95.54** | **92.22** | **95.54** | **92.22** | **95.54** | **92.22** |
| Feedstock handling | 8.91 | 8.91 | 8.91 | 8.91 | 8.91 | 8.91 |
| Belt dryer | 7.11 | 7.11 | 7.11 | 7.11 | 7.11 | 7.11 |
| ASU | 23.32 | 10.25 | 23.32 | 10.25 | 23.32 | 10.25 |
| $O_2$ compressor | 2.35 | 0.43 | 2.35 | 0.43 | 2.35 | 0.43 |
| Pressurized $O_2$ CFB gasifier | 29.58 | — | 29.58 | — | 29.58 | — |
| Steam CFB gasifier | — | 13.25 | — | 13.25 | — | 13.25 |
| Combustor with fuelgas treatment | — | 30.87 | — | 30.87 | — | 30.87 |
| Ceramic hot-gas filter | 6.99 | 6.17 | 6.99 | 6.17 | 6.99 | 6.17 |
| Catalytic reformer | 17.27 | 15.24 | 17.27 | 15.24 | 17.27 | 15.24 |
| **Syngas purification, conditioning and compression, M€** | **46.42** | **38.54** | **54.00** | **52.19** | **74.89** | **68.02** |
| Scrubber | 1.38 | 1.23 | 1.38 | 1.23 | 1.38 | 1.23 |
| Liquid redox | 2.90 | 2.58 | 2.90 | 2.58 | 2.90 | 2.58 |
| Syngas compressor 1 | 14.56 | 17.23 | 16.84 | 17.65 | 16.84 | 17.65 |
| Syngas compressor 2 | 7.49 | 7.48 | — | — | 7.49 | 7.48 |
| Activated carbon | 0.37 | 0.33 | 0.37 | 0.33 | 0.37 | 0.33 |
| Waste water treatment | 1.53 | 1.34 | 1.02 | 1.70 | 1.53 | 1.70 |
| WGS reactors | 5.30 | — | 31.48 | 28.70 | 31.48 | 28.70 |
| $CO_2$ removal pre-combustion (MDEA) | 12.89 | 8.35 | — | — | 12.89 | 8.35 |
| **Methanol and hydrogen production, M€** | **10.99** | **10.98** | **5.65** | **5.10** | **16.64** | **16.09** |
| Methanol synthesis BWR | 6.97 | 6.95 | — | — | 6.97 | 6.95 |
| Recycle compressor | 2.10 | 2.09 | — | — | 2.10 | 2.09 |
| Stabilizing column | 0.41 | 0.41 | — | — | 0.41 | 0.41 |
| Concentration column | 1.52 | 1.53 | — | — | 1.52 | 1.53 |
| PSA | — | — | 5.65 | 5.10 | 5.65 | 5.10 |
| **Heat recovery, M€** | **2.97** | **2.52** | **5.55** | **3.72** | **5.77** | **4.09** |
| CHP internal combustion engine | 1.29 | — | 3.03 | — | 3.03 | — |
| Boiler | — | 0.43 | — | 0.97 | — | 0.97 |
| Heat exchangers | 1.68 | 2.09 | 2.52 | 2.76 | 2.73 | 3.12 |
| **Total FCI without CCS, M€** | **155.91** | **144.26** | **160.74** | **153.25** | **192.83** | **180.42** |
| **$CO_2$ separation and compression, M€** | **18.69** | **41.83** | **49.83** | **65.52** | **36.94** | **57.17** |
| $CO_2$ removal pre-combustion (MDEA) | — | — | 18.44 | 15.16 | +5.56[b] | +6.81[b] |
| Decreased PSA cost[a] | — | — | −2.02 | −1.52 | −2.02 | −1.52 |
| $CO_2$ removal post-combustion (MEA) | 4.29 | 26.85 | 11.96 | 29.89 | 11.96 | 29.89 |
| $CO_2$ compression and dehydration unit | 14.40 | 14.98 | 21.44 | 21.99 | 21.44 | 21.99 |
| **Total FCI, M€** | **174.60** | **186.09** | **210.56** | **218.77** | **229.77** | **237.59** |

[a] $BtH_2$ plants without CCS include higher size PSA units because a higher amount of syngas needs to be treated when $CO_2$ is not separated by the MDEA process. The decreased cost of PSA when MDEA is added to the plant is taken into account. [b] In $BtMH_2$ plants, the MDEA unit is designed for methanol production without CCS and for hydrogen production with CCS. These values correspond to the incremental cost of the MDEA process when designed for hydrogen production rather than for methanol production.

 

the cost for $CO_2$ separation and additional compression sections for methanol production. The DG-based plants for methanol production show a higher syngas purification, conditioning and compression cost compared to the IG-based plants, because of the more complex syngas conditioning process and the higher flow rate of captured $CO_2$. The higher complexity of the methanol synthesis and purification island compared to the PSA unit leads to a higher cost of the methanol synthesis section compared to hydrogen purification. Again, the flexible $BtMH_2$ plants feature the highest capital investment cost, as they include the equipment for the delivery of both products. The heat recovery section is slightly more expensive in the DG-based plants due to the installation of a CHP internal combustion engine instead of a boiler.

The fixed capital investment (FCI) of plants without CCS can be approximately derived by summing up all the aforementioned cost items. The simplifying assumption is that without $CO_2$ scrubbing units, a different design of the heat recovery would likely be preferable and might include a steam cycle for power production. On the other hand, MDEA scrubbing cannot be avoided to reach the target module in the methanol production plants. The FCI of plants without CCS results in being lower in the methanol production plants and in the IG-based plants. When CCS is considered, MEA scrubbing, $CO_2$ capture and compression units in all the plants, and MDEA in $BtH_2$ plants must be added. In hydrogen production plants with CCS, MDEA technology is necessary to obtain a high-purity $CO_2$ stream not diluted with other compounds in the PSA off-gas. The capital costs increase from a minimum of 12% in BtM DG-based plants (174.6 *vs.* 155.9 M€) up to a maximum of 43% in the $BtH_2$ IG plants (218.8 *vs.* 153.2 M€). Overall, the IG-based plants with CCS have the highest FCI due to the larger size of the post-combustion $CO_2$ capture unit.

In the flexible $BtMH_2$ plants, the equipment for CCS represents about 16% and 24% of the FCI in the DG-based and IG-based plants respectively. The inclusion of the methanol synthesis process involves an increase of 9–14% of the FCI compared to the corresponding $BtH_2$ plants.

Table 10 shows the main results of the economic analysis based on the levelized cost approach. The multi-product plants are assumed to be operated for 50% of the time in methanol production mode and 50% of the time in hydrogen mode. Most of the product cost is associated with capex (40–43% of the total cost), followed by O&M (29–31%) and biomass purchase (17–22%). Electricity and $CO_2$ transport and storage have a much lower impact on the production costs (3–6% each). The methanol production plants show the lowest yearly total costs, followed by the hydrogen production plants and the flexible multi-product plants. The hydrogen production plants show the highest $CO_2$ transport and storage cost because of the highest amount of $CO_2$ separated. The methanol production plants are characterized by lower LCOF, followed by the hydrogen production plants and the multi-product plants. By considering the same final product, the DG-based plants result in lower LCOF. Compared to the bio-hydrogen plant assessed by Hannula *et al.*,[9] who estimated a hydrogen cost of 42.2 € per GJ (Table 1), 13% lower LCOF has been obtained in this work for the $BtH_2$ DG plant, mainly due to the fact that Hannula *et al.* referred to a first-of-a-kind (FOAK) plant, involving a higher total capital investment than that in this work, that refers to $N^{th}$-of-a-kind (NOAK) cost assumptions.

Fig. 5 shows the marginal $CO_2$ avoidance cost *vs.* the captured $CO_2$ in the DG- and IG-based plants respectively. In the DG-based plants, about 5% of the $CO_2$ is avoided at zero marginal cost and stored in the unconverted biochar. The horizontal lines on the left hand side of the graph represent the marginal cost of adding CCS to a biomass-to-X plant (*i.e.* adding the $CO_2$ compression unit in the methanol production plant and adding MDEA scrubbing and $CO_2$ compression in the hydrogen production plant). On the right hand side, the step increase represents the marginal cost of adding the post-combustion MEA scrubbing unit and the corresponding $CO_2$ compression.

In the plot, the following assumptions are adopted for the sake of simplicity: (i) the scale effects on the capital cost of the equipment for $CO_2$ capture, transport and storage are not taken into account (if more $CO_2$ is captured, the $CO_2$ avoidance cost should decrease, generating declining lines instead of horizontal ones); (ii) the absence of MDEA and MEA units would favor heat integration of the plant with a steam cycle for power production, affecting the economics of the plants without $CO_2$ capture or with partial capture.

In the BtM DG plant, a $CO_2$ capture rate of 54.7% is reached at a cost of 40.8 € per $t_{CO_2}$ through compression (27.4 € per $t_{CO_2}$) and transport and storage (13.4 € per $t_{CO_2}$). By adding the MEA post-combustion capture unit and increasing the $CO_2$

Table 10 Main results of the economic analysis and levelized cost of fuel

| Economic results | BtM DG | BtM IG | $BtH_2$ DG | $BtH_2$ IG | $BtMH_2$ DG | $BtMH_2$ IG |
|---|---|---|---|---|---|---|
| TCI CCF, M€ per y | 24.12 | 25.71 | 29.09 | 30.22 | 31.74 | 32.82 |
| O&M, M€ per y | 17.71 | 18.82 | 20.82 | 21.76 | 22.51 | 23.36 |
| Purchased electricity cost, M€ per y | 3.01 | 3.74 | 2.29 | 3.78 | 2.65 | 3.76 |
| $CO_2$ transport and storage cost, M€ per y | 2.10 | 2.23 | 3.81 | 3.95 | 2.95 | 3.09 |
| Biomass cost, M€ per y | 13.32 | 13.32 | 13.32 | 13.32 | 13.32 | 13.32 |
| Total cost, M€ per y | 60.27 | 63.81 | 69.33 | 73.03 | 73.18 | 76.35 |
| Methanol production, t $year^{-1}$ | 92 823 | 93 822 | — | — | 46 412 | 46 911 |
| Hydrogen production, t $year^{-1}$ | — | — | 16 006 | 16 214 | 8003 | 8107 |
| LCOF, € per t | 649 | 680 | 4331 | 4505 | — | — |
| LCOF, € per GJ | 32.63 | 34.18 | 36.07 | 37.51 | 38.83 | 40.03 |

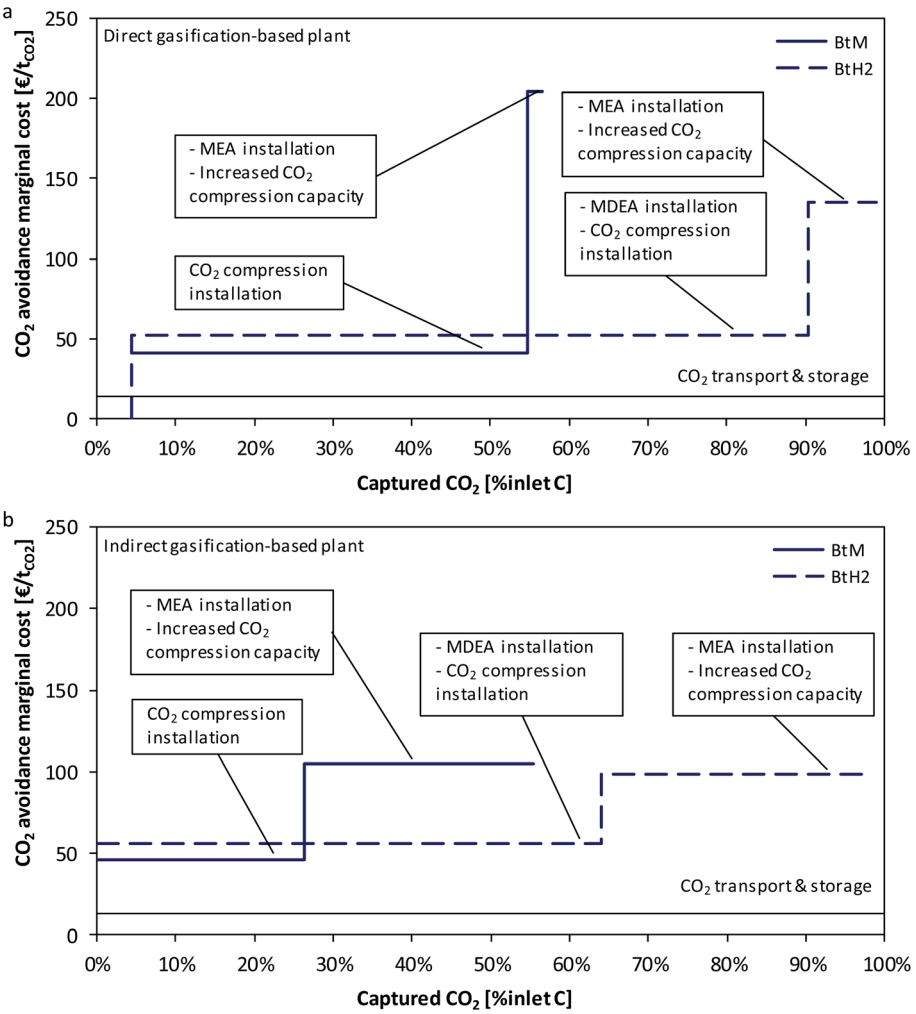


Fig. 5 $CO_2$ avoidance marginal cost *vs.* captured $CO_2$ in DG-based plants (a) and in IG-based plants (b). In DG-based plants, 4.5% of the inlet carbon is stored as biochar.

compression capacity, the $CO_2$ capture rate is increased by 1.8% at a marginal cost of 204.9 € per $t_{CO_2}$. In the $BtH_2$ DG plant, a $CO_2$ capture rate of 90.30% is reached at a cost of 52.2 € per $t_{CO_2}$ (38.8 € per $t_{CO_2}$ for capture + 13.4 € per $t_{CO_2}$ for transport and storage). The marginal cost of adding post-combustion $CO_2$ capture and increasing the capture rate up to 99% is 135.3 € per $t_{CO_2}$.

In BtM IG plants, a $CO_2$ capture rate of 26.3% is reached at a cost of 45.8 € per $t_{CO_2}$ (32.4 € per $t_{CO_2}$ for capture + 13.4 € per $t_{CO_2}$ for transport and storage), through the addition of compressors for the $CO_2$ separated by the MDEA unit. By adding the MEA post-combustion capture unit and increasing the $CO_2$ compression capacity, the $CO_2$ capture rate is increased by 29% at a marginal cost of 105.1 € per $t_{CO_2}$. In $BtH_2$ IG plants, a $CO_2$ capture rate of 64% is reached at 55.6 € per $t_{CO_2}$ by integrating the MDEA separation process and $CO_2$ compression (42.2 € per $t_{CO_2}$ for capture + 13.4 € per $t_{CO_2}$ for transport and storage). The addition of the MEA plant and the increase of the $CO_2$ compression unit allows the increase of the capture rate up to 98.1%, at a marginal cost of 98.4 € per $t_{CO_2}$. Post-combustion MEA scrubbing is needed in IG-based plants to reach high $CO_2$ capture rates.

BECCS plants benefit from $CO_2$ credits that reward their capacity to remove $CO_2$ from the atmosphere. Fig. 6 shows the LCOF as a function of the $CO_2$ credits for plants with no CCS, partial CCS (CCSp, achieved *via* $CO_2$ compression in BtM, and $CO_2$ separation and compression in $BtH_2$ plants) and maximum CCS (CCSm, achieved *via* MEA-based $CO_2$ separation and increased $CO_2$ compression capacity).

The BtM DG plant (Fig. 6a) needs 40.84 € per $t_{CO_2}$ and 46.76 € per $t_{CO_2}$ in CCSp and CCSm cases respectively to reach a production cost of 28.66 € per GJ in the case without CCS. The two CCS configurations show a very similar trend of the LCOF in the selected $CO_2$ credit range since they capture a very similar amount of $CO_2$. The BtM IG plant (Fig. 6b) requires 45.76 and 76.87 € per $t_{CO_2}$ in CCSp and CCSm cases respectively to reach a production cost of 27.33 € per GJ in the case with no CCS. For $CO_2$ credits higher than 105.1 € per $t_{CO_2}$ (*i.e.* the marginal cost to achieve the highest capture rate), the CCSm configuration becomes economically more competitive than the CCSp case.

 

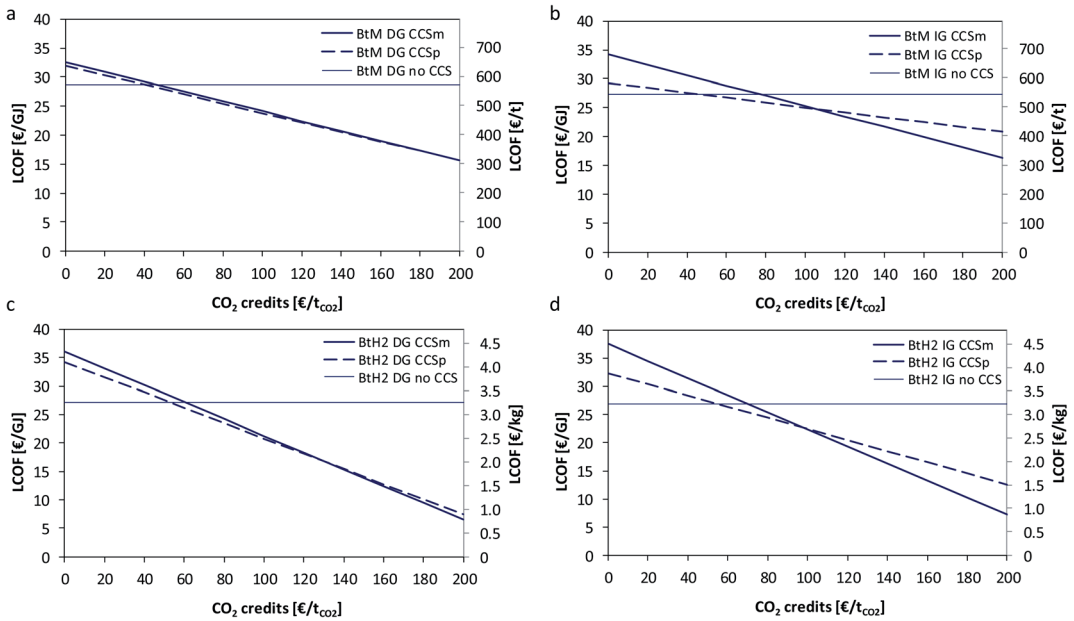


Fig. 6 LCOF *vs.* $CO_2$ credits of BECCS plants: (a) BtM DG, (b) BtM IG, (c) $BtH_2$ DG, and (d) $BtH_2$ IG. CCSp: installation of $CO_2$ compression. CCSm: installation of MEA and increase of $CO_2$ compression capacity.

The $BtH_2$ DG plant (Fig. 6c) must be rewarded with 52.23 and 59.85 € per $t_{CO_2}$ in CCSp and CCSm respectively to achieve 27.22 € per GJ in the case without CCS. $CO_2$ credits of 135.3 € per $t_{CO_2}$ makes the CCSm configuration more competitive than CCSp. The $BtH_2$ IG plant (Fig. 6d) needs 55.63 and 70.48 € per $t_{CO_2}$ in CCSp and CCSm respectively to reach the same LCOF of 26.83 € per GJ as the case with no CCS. $CO_2$ credits of 98.4 € per $t_{CO_2}$, which is again equal to the marginal cost for maximum capture, are necessary to make CCSm the most competitive case.

It is also worth observing that hydrogen production plants show steeper lines compared to methanol plants thanks to the higher amount of captured $CO_2$ per GJ of the delivered product. Therefore, $BtH_2$ plants become economically favourable at higher $CO_2$ credits.

In CCSm cases, $CO_2$ credits of 148 € per $t_{CO_2}$ for DG-based and 158 € per $t_{CO_2}$ for IG-based allow a methanol production cost of around 400 € per t (*i.e.* 20.1 € per GJ) to be achieved and credits of 131 € per $t_{CO_2}$ for DG-based and 138 € per $t_{CO_2}$ for IG-based allow $H_2$ production costs of 2 € per kg (*i.e.* 16.7 € per GJ) to be achieved.

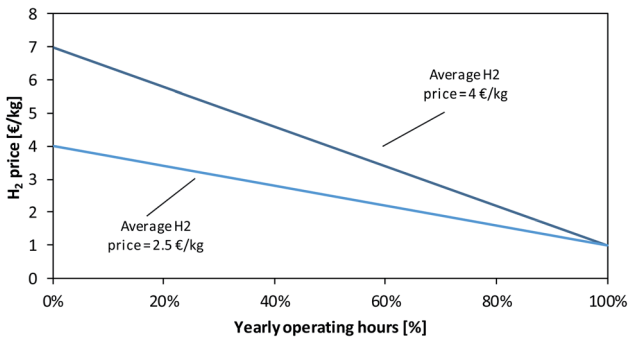


Fig. 7 Yearly hydrogen selling price profiles.

As previously mentioned, in a context where the expected time-dependent relative value of power, carbon-based products, hydrogen, and sequestered $CO_2$ determines a significant variation in the revenues of bioenergy plants, multi-product plants that can be operated flexibly to produce the goods with the highest added value may gain an economic advantage. For a simplified economic analysis of a flexible methanol and $H_2$ plant, three different methanol selling prices (*i.e.* 450, 550, and 650 € per t) are selected and assumed to remain constant throughout the year. Two simple linear profiles are assumed for the cumulative hydrogen selling price (see Fig. 7), ranging between a high price of 7 € per kg or 4 € per kg, representative of periods with low availability of renewable electricity and green $H_2$, and a low price of 1 € per kg, representative of periods with high availability of renewable electricity and green $H_2$. These two scenarios involve an average yearly $H_2$ market price of 4 and 2.5 € per kg. The rationale behind the assumption of a hydrogen price profile is that water electrolysis is expected to become the leading technology for hydrogen production in the long-period. Therefore, the breakeven hydrogen selling price will be influenced by the electricity price, inheriting its volatility, possibly shrunk by some degree depending on the availability and cost of $H_2$ storage. $CO_2$ credits of 120 € per $t_{CO_2}$ are assumed for the stored $CO_2$ in these calculations.

In Fig. 8a and b, the internal rate of return (IRR) of the flexible multi-product plants producing methanol and hydrogen is compared with the IRR of methanol and hydrogen plants delivering a single-product. On the *x*-axis, the fraction of hours in which the plants operate producing hydrogen is reported. Methanol plants are depicted as points on the left

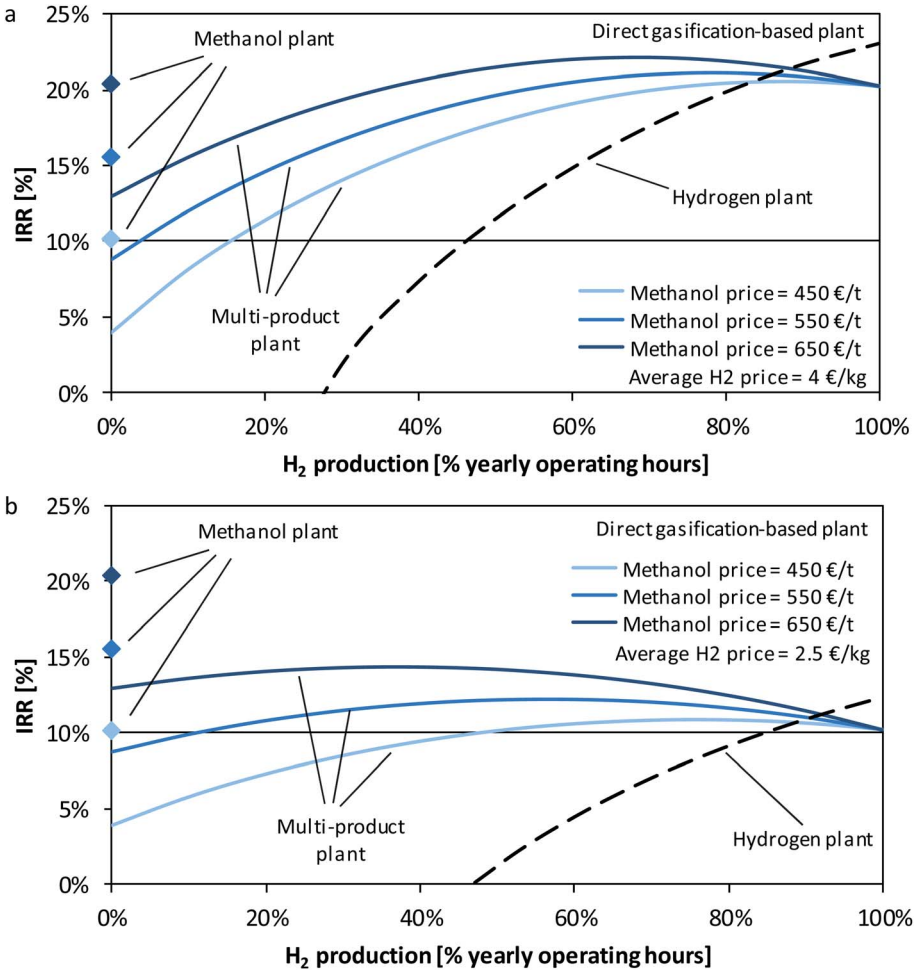


Fig. 8 IRR *vs.* yearly operating hours in hydrogen production mode: (a) yearly average $H_2$ price = 4 € per kg and (b) yearly average $H_2$ price = 2.5 € per kg.

ordinate axis, since they never produce hydrogen. The hydrogen plant curve shows an increasing trend with the yearly operating hours. Therefore, 100% of the yearly operating hours corresponds to the optimal conditions. It has to be noted that the optimal number of operating hours could be lower than 100%, in case the operational costs (biomass and power purchase, variable O&M) overtake the hydrogen selling price, making the interruption of the plant operation economically convenient. For a specified methanol price, the maximum IRR obtained by the multi-product plant must be compared with the highest IRR found on the hydrogen production plant curve and the value achieved by the methanol plant for that assumed price. As shown in Fig. 8a, for methanol selling prices of 650, 550 and 450 € per t, the economic optimum of the multi-product plant is achieved when it operates for about 70, 80 and 90% of the time in hydrogen mode and the remaining hours in methanol mode. IRRs of 22.1, 21.1 and 20.5% are higher than the optimal values generated by the single-product methanol plants (*i.e.* 20.4, 15.5 and 10.2%), but lower than the optimal value generated by the single-product hydrogen plant (*i.e.* 23%).

Considering the lower hydrogen price scenario (Fig. 8b), for the maximum methanol selling price curve (*i.e.* 650 € per t), the multi-product plant should operate for about 40% of the time in hydrogen mode and the remaining hours in methanol mode. In this case, the IRR of 14.3% is higher than the optimal value generated by the single-product hydrogen plant (*i.e.* 12.3%), but lower than the value generated by the single-product methanol plant (*i.e.* 20.4%). Considering lower methanol selling prices (*i.e.* 550 and 450 € per t), the multi-product plant should operate for 60% and 80% of the yearly operating hours in hydrogen mode. In this case, the IRRs of 12.2% and 10.8%, for the 550 and 450 € per t methanol prices respectively, are lower than the hydrogen single-product plant, but at least for the 450 € per t higher than the single-product methanol plant.

Overall, with the assumptions of this study, multi-product plants result in a slightly higher or slightly lower IRR than the single-product plants with the highest revenues. On the other hand, they are never the worst case scenario despite the highest investment costs, thus offering a potential advantage from the financial risk perspective thanks to lower exposure to market price volatility.

 

# 5. Conclusions

In this work, a techno-economic analysis of biomass-to-methanol and biomass-to-hydrogen plants with CCS has been carried out. Each plant is studied including either oxygen-blown direct gasification (DG) or air-blown dual fluidized bed indirect gasification (IG). MDEA and MEA-based solvent scrubbing are considered as $CO_2$ removal technologies from syngas and flue gas respectively. These solutions have been compared in terms of fuel efficiency and carbon recovery potential. The economic impact of adding CCS and of increasing the amount of $CO_2$ which is captured within the plants is investigated together with the impact of $CO_2$ credits on the overall economics of the plants.

A third solution involving multi-product bioenergy plants able to flexibly produce methanol or hydrogen depending on the relative selling price is hence introduced in the analysis.

The main conclusions can be summarised as follows:

- In DG-based plants, most of the $CO_2$ is captured from syngas with MDEA solvent (50% and 86% of the inlet carbon for methanol and hydrogen production, respectively) and a much lower amount of $CO_2$ is captured from flue gas with MEA (2% and 9% for methanol and hydrogen production, respectively). Conversely, in IG-based plants, MEA is necessary to achieve high $CO_2$ capture efficiency, as 27% of the total inlet carbon is captured from the IG combustor and between 2% and 7% of $CO_2$ is separated from the flue gas of the tail gas boiler. Because of the high heat demand for $CO_2$ separation in IG cases, plants have been designed without a heat recovery steam cycle. In this way the heat available for solvent regeneration is maximized, penalizing the electricity balance.

- The maximum $CO_2$ capture rate achieved is 55–57% in methanol production plants and 98–99% in hydrogen production plants. The capture rate in methanol plants is lower than that in hydrogen plants, as part of the inlet carbon is stored in the product. In all the assessed cases, less than 2% of the inlet carbon is vented to the atmosphere as $CO_2$.

- The overall fuel efficiencies are slightly higher in hydrogen plants (67.6–68.5%) than in methanol plants (65.1–65.8%), with a minor dependency on the gasification technology. The obtained values are in the high range of the fuel efficiency intervals reported in the literature.

- Methanol production plants are characterized by lower LCOF (referred to the LHV energy output) than hydrogen plants: 32.6–34.2 € per GJ (or 649–680 € per t) *vs.* 36.1–37.5 € per GJ (or 4.3–4.5 € per kg), with zero revenues from $CO_2$ storage. This is mainly due to the higher cost for $CO_2$ capture in hydrogen plants, where higher amounts of $CO_2$ are separated and compressed. By considering the same final product, the DG-based plants show slightly lower LCOF (32.6–36.1 € per GJ *vs.* 34.2–37.1 € per GJ), mainly thanks to the lower $CO_2$ separation cost.

- In methanol production plants, a $CO_2$ capture rate of up to 55 and 26% can be reached at marginal costs of 41 and 46 € per $t_{CO_2}$ for DG- and IG-based plants respectively (including 13.4 € per $t_{CO_2}$ for $CO_2$ transport and storage). Such relatively low costs are associated with the compression (27–32 € per $t_{CO_2}$) and transport and storage (13.4 € per $t_{CO_2}$) costs, as $CO_2$ separation from syngas is anyway needed to produce syngas tailored for methanol synthesis. By adding MEA-based post-combustion capture and increasing the size of the $CO_2$ compression unit, the $CO_2$ capture rate is increased by $2\%_{pt}$ and $29\%_{pt}$ at a marginal cost of 205 and 105 € per $t_{CO_2}$ for DG- and IG-based plants respectively. A similar figure is obtained for the hydrogen plants, where the addition of MDEA-based $CO_2$ separation (not needed in plants without CCS) allows achieving a $CO_2$ capture rate of 90% and 64% at a cost of 52 and 56 € per $t_{CO_2}$ for DG- and IG-based plants respectively. By adding post-combustion capture units and increasing the $CO_2$ compression unit size, the $CO_2$ capture rate can be increased up to 99 and 98% at a marginal cost of 135 and 98 € per $t_{CO_2}$ for DG- and IG-based plants respectively.

- When credits for $CO_2$ storage are included, a breakeven price of 47–77 € per $t_{CO_2}$ makes the plants with the maximum $CO_2$ capture rate competitive with the corresponding plants without CCS. $CO_2$ credits of 148–158 € per $t_{CO_2}$ allow methanol production costs of around 400 € per t to be achieved and credits of 131–138 € per $t_{CO_2}$ allow $H_2$ production costs of 2 € per kg to be achieved. Because of the higher amount of captured $CO_2$ per unit of product output, $H_2$ production plants obtain higher economic benefits from higher $CO_2$ storage credits.

- Multi-product plants flexibly producing methanol and hydrogen results in the highest capital costs (+9–14% than the corresponding $H_2$ production plant) and the highest LCOF. However, with the assumptions adopted in this work (fixed methanol selling price varied between 450 and 650 € per t and time dependent $H_2$ selling price between 1 and 4 or 7 € per kg), the internal rate of return of the flexible methanol + $H_2$ plants is slightly higher or slightly lower than the corresponding single-product plant with the highest revenues. On the other hand, multi-product flexible plants are never the worst case scenario despite the highest investment costs, thus offering a potential advantage from the financial risk perspective thanks to lower exposure to market price volatility.

It has to be noted that methanol has been selected in this work as a representative high value carbon-based product. As for the flexible multi-product plants, we are confident that the obtained conclusions will qualitatively hold also if other carbon-based bioproducts such as methane or Fischer–Tropsch liquids are considered.

Moreover, this study assumed that flexible plants are operated either in hydrogen production or in methanol production mode. However, operating points involving co-production of hydrogen and methanol may be possible and may be preferable in real plants to improve the dynamic performance in the transient between different operating points. The optimal process design and operating criteria of real plants will also depend on the expected switching frequency between different operating modes, which, in turn, will depend on the local market conditions in which the plant is located.

# Author contributions

A. Poluzzi: conceptualization, methodology, investigation, formal analysis, writing – original draft, visualization, and

writing – review & editing. G. Guandalini: conceptualization, methodology and validation. M. C. Romano: conceptualization, supervision, methodology, validation, and writing – review & editing.

## Conflicts of interest

There are no conflicts of interest to declare.

## Abbreviation

**Acronyms**

| | |
|---|---|
| ASU | Air separation unit |
| ATR | Autothermal reformer |
| BECCS | Bioenergy with carbon capture and storage |
| BFB | Bubbling fluidized bed |
| $BtH_2$ | Biomass-to-hydrogen |
| BtM | Biomass-to-methanol |
| $BtMH_2$ | Biomass-to-methanol and hydrogen |
| BtX | Biomass-to-X |
| BWR | Boiling water reactor |
| CCS | Carbon capture and storage |
| CFB | Circulating fluidized bed |
| CZA | Methanol synthesis catalyst $Cu/ZnO/Al_2O_3$ |
| DME | Dimethyl ether |
| GHSV | Gas hourly space velocity |
| ICE | Internal combustion engine |
| LHV | Lower heating value |
| RR | Recycle ratio |
| SEG | Sorption-enhanced gasification |
| WGS | Water gas shift |

**Symbols**

| | |
|---|---|
| $C_{\text{feedstock}}$ | Cost of feedstock |
| $C_{\text{fixed O\&M}}$ | Fixed O&M cost |
| $C_{\text{ut}}$ | Utilities cost |
| $C_{\text{tot}}$ | Total cost |
| CE | Carbon efficiency |
| CCF | Capital charge factor |
| $F_{\text{C,biom}}$ | Carbon molar flow rate in the inlet biomass |
| $F_{\text{C,stored}}$ | Carbon molar flow rate for storage |
| $F_{\text{i}}$ | Component –i molar flow rate |
| $F_{\text{M}}$ | Methanol molar flow rate |
| FCI | Fixed capital investment |
| $h_{\text{eq}}$ | Equivalent yearly operating hours |
| IRR | Internal rate of return |
| LCOF | Levelized cost of fuel |
| LT | Plant lifetime |
| $\dot{m}$i | Component –i mass flow rate |
| $M_{\text{tot}}$ | Amount of fuel |
| $P_{\text{el}}$ | Net electric output |
| $p_{\text{i}}$ | Partial pressure –i |
| $R$ | Reduction factor |
| TCI | Total capital investment cost |
| $\eta_{\text{el,ref}}$ | Reference steam cycle electric efficiency |
| $\eta_{F,\text{dryer}}$ | Dryer fuel efficiency |
| $\eta_{F,gas}$ | Gasifier fuel efficiency |
| $\eta_{F,\text{ref}}$ | Reformer fuel efficiency |
| $\eta_{F,\text{pur-co}}$ | Purification and conditioning fuel efficiency |
| $\eta_{F,\text{syn}}$ | Methanol synthesis fuel efficiency |
| $\eta_{F,\text{f\_pur}}$ | Fuel purification fuel efficiency |
| $\eta_{F,\text{global}}$ | Global fuel efficiency |
| $\eta_{F,\text{eq}}$ | Equivalent fuel efficiency |



## Acknowledgements

Lorenzo Baggi and Matteo Catania are acknowledged for the preliminary work carried out in their MSc thesis on flexible biomass to methanol and hydrogen plants.

## References

1 S. E. Baker, J. K. Stolaroff, G. Peridas, S. H. Pang, H. M. Goldstein, F. R. Lucci, W. Li, E. W. Slessarev, J. Pett-Ridge, F. J. Ryerson, J. L. Wagoner, W. Kirkendall, R. D. Aines, D. L. Sanchez, B. Cabiyo, J. Baker, S. McCoy, S. Uden, R. Runnebaum, J. Wilcox, P. C. Psarras, H. Pilorgé, N. McQueen, D. Maynard and C. McCormick, *Getting to Neutral: Options for Negative Carbon Emissions in California*, 2020.

2 M. Bui, M. Fajardy, D. Zhang and N. Mac Dowell, *Delivering Negative Emissions From Biomass Derived Hydrogen H2FC Supergen White Paper*, 2020, pp. 1–81.

3 I. Hannula and D. M. Reiner, Near-Term Potential of Biofuels, Electrofuels, and Battery Electric Vehicles in Decarbonizing Road Transport, *Joule*, 2019, **3**, 2390–2402.

4 International Energy Agency, *Energy Technology Perspectives*, OECD, 2017.

5 E. D. Larson, H. Jin and F. E. Celik, Large-scale gasification-based coproduction of fuels and electricity from switchgrass, *Biofuels, Bioprod. Biorefin.*, 2009, **3**, 174–194.

6 Y. K. Salkuyeh, B. A. Saville and H. L. MacLean, Techno-economic analysis and life cycle assessment of hydrogen production from different biomass gasification processes, *Int. J. Hydrogen Energy*, 2018, **43**, 9514–9528.

7 C. Antonini, K. Treyer, E. Moioli, C. Bauer, T. J. Schildhauer and M. Mazzotti, Hydrogen from wood gasification with CCS – a techno-environmental analysis of production and use as transport fuel, *Sustainable Energy Fuels*, 2021, **5**, 2602–2621.

8 C. Arnaiz del Pozo, S. Cloete and Á. J. Álvaro, Carbon-negative hydrogen: Exploring the techno-economic potential of biomass co-gasification with $CO_2$ capture, *Energy Convers. Manage.*, 2021, **247**, 114712.

9 I. Hannula and K. Melin, *Biorefineries with CCS IEAGHG Technical Report*, 2021.

10 A. Poluzzi, G. Guandalini, F. d'Amore and M. C. Romano, The Potential of Power and Biomass-to-X Systems in the Decarbonization Challenge: a Critical Review, *Curr. Sustainable/Renewable Energy Rep.*, 2021, **8**, 242–252.

11 A. Poluzzi, G. Guandalini, S. Guffanti, C. Elsido, S. Moioli, P. Huttenhuis, G. Rexwinkel, E. Martelli, G. Groppi and

 

M. C. Romano, Flexible Power & Biomass-to-Methanol plants: Design optimization and economic viability of the electrolysis integration, *Fuel*, 2022, **310**, 122113.

12 A. Poluzzi, G. Guandalini, S. Guffanti, M. Martinelli, S. Moioli, P. Huttenhuis, G. Rexwinkel, J. Palonen, E. Martelli, G. Groppi and M. C. Romano, Flexible Power and Biomass-To-Methanol Plants With Different Gasification Technologies, *Front. Energy Res.*, 2022, **9**, 795673.

13 T. Pröll and H. Hofbauer, $H_2$ rich syngas by selective $CO_2$ removal from biomass gasification in a dual fluidized bed system - Process modelling approach, *Fuel Process. Technol.*, 2008, **89**, 1207–1217.

14 A. Giuffrida, M. C. Romano and G. G. Lozza, Thermodynamic assessment of IGCC power plants with hot fuel gas desulfurization, *Appl. Energy*, 2010, **87**, 3374–3383.

15 E. Kurkela, M. Kurkela, C. Frilund, I. Hiltunen, B. Rollins and A. Steele, Flexible Hybrid Process for Combined Production of Heat, Power and Renewable Feedstock for Refineries: Managing seasonal energy supply and demand for heat and power in Europe, *Johnson Matthey Technol. Rev.*, 2021, **65**, 333–345.

16 B. Echt, D. Leppin, D. Mamrosh, D. Mirdadian, D. Seeger, B. Warren, Fundamentals of Low-Tonnage Sulfur Removal and Recovery, *Presented at the Laurance Reid Gas Conditioning Conference*, Norman (OK), 2017, pp. 1–99.

17 A. Kazemi, M. Malayeri, A. Gharibi kharaji and A. Shariati, Feasibility study, simulation and economical evaluation of natural gas sweetening processes - Part 1: A case study on a low capacity plant in Iran, *J. Nat. Gas Sci. Eng.*, 2014, **20**, 16–22.

18 H. Hiller, R. Reimert, F. Marschner, H.-J. Renner, W. Boll, E. Supp, M. Brejc, W. Liebner, G. Schaub, G. Hochgesand, C. Higman, P. Kalteier, W.-D. Müller, M. Kriebel, H. Schlichting, H. Tanz, H.-M. Stönner, H. Klein, W. Hilsebein, V. Gronemann, U. Zwiefelhofer, J. Albrecht, C. J. Cowper and H. E. Driesen, Gas Production, *Ullmann's Encycl. Ind. Chem.*, 2006.

19 I. Hannula and E. Kurkela, Liquid Transportation Fuels *via* Large-Scale Fluidised Bed Gasification of Lignocellulosic Biomass, *VTT Technology 91*, 2013.

20 P. Brandl, M. Bui, J. P. Hallett and N. Mac Dowell, Beyond 90% capture: Possible, but at what cost?, *Int. J. Greenhouse Gas Control*, 2021, **105**, 103239.

21 K. M. Vanden Bussche and G. F. Froment, A Steady-State Kinetic Model for Methanol Synthesis and the Water Gas Shift Reaction on a Commercial $Cu/ZnO/Al_2O_3$ Catalyst, *J. Catal.*, 1996, **161**, 1–10.

22 Aspentech, *Aspen Plus Methanol Synthesis Model*, 2018.

23 D.-W. Lee, M. S. Lee, J. Y. Lee, S. Kim, H.-J. Eom, D. J. Moon and K.-Y. Lee, The review of Cr-free Fe-based catalysts for high-temperature water-gas shift reactions, *Catal. Today*, 2013, **210**, 2–9.

24 J. Stöcker, M. Whysall, G. Q. Miller, *30 Years of PSA Technology for Hydrogen Purification*, UOP LLC, 1998, pp. 1–25.

25 R. E. Meissner and U. Wagner, Low-energy process recovers $CO_2$, *Oil Gas J.*, 1983, 55–58.

26 S. Moioli, A. Giuffrida, M. C. Romano, L. A. Pellegrini and G. Lozza, Assessment of MDEA absorption process for sequential H2S removal and CO2 capture in air-blown IGCC plants, *Appl. Energy*, 2016, **183**, 1452–1470.

27 S. Moioli, L. A. Pellegrini, M. C. Romano and A. Giuffrida, Pre-combustion CO2 Removal in IGCC Plant by MDEA Scrubbing: Modifications to the Process Flowsheet for Energy Saving, *Energy Procedia*, 2017, **114**, 2136–2145.

28 J. Gale, Understanding the Cost of Retrofitting $CO_2$ capture in an Integrated Oil Refinery, *IEAGHG Technical Review*, 2017.

29 G. Collodi, G. Azzaro and N. Ferrari, Techno - Economic Evaluation of SMR Based Standalone (Merchant) Hydrogen Plant with CCS, *IEAGHG Technical Report 2017-02*, 2017.

30 M. Zatti, M. Gabba, M. Rossi, M. Morini, A. Gambarotta and E. Martelli, Towards the optimal design and operation of multi-energy systems: the 'efficity' project, *Environ. Eng. Manage. J.*, 2018, **17**, 2409–2419.

31 H. J. Grabke, Metal Dusting of Low- and High-Alloy Steels, *Corrosion*, 1995, **51**, 711–720.

32 P. E. Queneau and S. W. Marcuson, Oxygen pyrometallurgy at copper cliff—A half century of progress, *JOM*, 1996, **48**, 14–21.